REPORT DOCUMENTATION PAGE

Form Approved OMB NO. 0704-0188

1. REPORT DATE (DD-MM-YYYY)	2. REPORT TYPE	3. DATES COVERED (From - To)
19-12-2014	Ph.D. Dissertation	-

4. TITLE AND SUBTITLE

Assessing Effects of Oxidizer Characteristics on Composite Reaction Kinetics

5a. CONTRACT NUMBER
W911NF-11-1-0439

5b. GRANT NUMBER

5c. PROGRAM ELEMENT NUMBER
611102

6. AUTHORS
Oliver Mulamba, Michelle Pantoya

5d. PROJECT NUMBER

5e. TASK NUMBER

5f. WORK UNIT NUMBER

7. PERFORMING ORGANIZATION NAMES AND ADDRESSES
Texas Technical University
Box 41035
349 Admin Bldg
Lubbock, TX 79409 -1035

8. PERFORMING ORGANIZATION REPORT NUMBER

9. SPONSORING/MONITORING AGENCY NAME(S) AND ADDRESS (ES)
U.S. Army Research Office
P.O. Box 12211
Research Triangle Park, NC 27709-2211

10. SPONSOR/MONITOR'S ACRONYM(S)
ARO

11. SPONSOR/MONITOR'S REPORT NUMBER(S)
58857-EG.49

12. DISTRIBUTION AVAILIBILITY STATEMENT
Approved for public release; distribution is unlimited.

13. SUPPLEMENTARY NOTES
The views, opinions and/or findings contained in this report are those of the author(s) and should not contrued as an official Department of the Army position, policy or decision, unless so designated by other documentation.

14. ABSTRACT
Enhancing the performance and efficiency of energetic materials is what helps to keep our military on the forefront of cutting edge weapon research and advancements. Whether it's increasing the energetic output, improving burn rates or decreasing sensitivity, the ability to tailor materials to a specified goal provides a foundation for continued improvements. This body of work investigates and assesses the effects of oxygen scavenging additives, varying molecular composition, and fragmental reactions on the reaction kinetics and thermal behaviors of different energetic compositions.

15. SUBJECT TERMS
iodine, alumnum, halogenated oxides, reactions, energy generation, differential scanning calorimetry, thermal gravimetric analysis, flame speeds, SEM, TEM, exothermic surface chemistry, alumina, pre ignition reaction

16. SECURITY CLASSIFICATION OF:			17. LIMITATION OF ABSTRACT	15. NUMBER OF PAGES	19a. NAME OF RESPONSIBLE PERSON
a. REPORT	b. ABSTRACT	c. THIS PAGE			Michelle Pantoya
UU	UU	UU	UU		19b. TELEPHONE NUMBER 806-742-3563

Report Title

Assessing Effects of Oxidizer Characteristics on Composite Reaction Kinetics

ABSTRACT

Enhancing the performance and efficiency of energetic materials is what helps to keep our military on the forefront of cutting edge weapon research and advancements. Whether it's increasing the energetic output, improving burn rates or decreasing sensitivity, the ability to tailor materials to a specified goal provides a foundation for continued improvements. This body of work investigates and assesses the effects of oxygen scavenging additives, varying molecular composition, and fragmental reactions on the reaction kinetics and thermal behaviors of different energetic compositions.

Closing the gap between practical and theoretical heat of combustion values requires innovative strategies for exploiting reaction kinetics. One potential strategy forcing reaction between Al and CuO, bypassing environmental oxygen is shown here to improve heat of combustion measurements significantly. Results reveal that using hafnium hydride additives at 10 mass% enhanced the heat of combustion of Al+CuO by 12%. The transition of this equilibrium based observation to a non-equilibrium fast heating setup is also investigated using plate deformation tests. Exploding bridge wire heads (EBW) initiated by a capacitive discharge unit (CDU) are used to dent plates and the deformation energies are estimated to observe the effects of varying composites in a non-equilibrium setting. The presence of HfH2 showed improved deformation energies for Al+CuO in the 10%.mass HfH2 range.

Taking polytetrafluoroethylene (PTFE) varying in chain lengths and molecular weight combined with the exothermic surface chemistry of the alumina passivation shell presents results based on very tailorable parameters. Experimentation was performed using simultaneous thermal analysis (STA) that covers both heat flow and mass loss. Flame speeds were also tested and required the use of an altered Bockmon tube method. Results showed a pre-ignition reaction (PIR) with longer chained PTFE samples and not with the shorter chained PTFE samples. The PIR is attributed to fluorine dislodging the hydroxyls from the alumina (Al2O3) surface and forming Al-F structures on the surface of Al2O3. Composites exhibiting the PIR correspondingly result in significantly higher flame speeds. The PIR surface chemistry may contribute to promoting the melt dispersion mechanism (MDM) responsible for propagating energy in nano Al reactions.

Assessing Effects of Oxidizer Characteristics on Composite Reaction Kinetics

By

Oliver K. Mulamba, MSME

A Dissertation

In

Mechanical Engineering

Submitted to the Graduate Faculty
of Texas Tech University in
Partial Fulfillment of
the Requirements for
the Degree of

DOCTOR OF PHILOSOPHY

Approved

Dr. Michelle Pantoya
Chair of Committee

Dr. Jharna Chaudhuri

Dr. Stephen Ekwaro-Osire

Dr. Todd Anderson

Dr. Andrew Jackson

Interim Dean of the Graduate School

December, 2013

ACKNOWLEDGMENTS

I gratefully acknowledge support from the Army Research Office under contract W911NF1110439 and encouragement from our Program Manager, Dr. Ralph Anthenien.

TABLE OF CONTENTS

ABSTRACT

Enhancing the performance and efficiency of energetic materials is what helps to keep our military on the forefront of cutting edge weapon research and advancements. Whether it's increasing the energetic output, improving burn rates or decreasing sensitivity, the ability to tailor materials to a specified goal provides a foundation for continued improvements. This body of work investigates and assesses the effects of oxygen scavenging additives, varying molecular composition, and fragmental reactions on the reaction kinetics and thermal behaviors of different energetic compositions.

Closing the gap between practical and theoretical heat of combustion values requires innovative strategies for exploiting reaction kinetics. One potential strategy forcing reaction between Al and CuO, bypassing environmental oxygen is shown here to improve heat of combustion measurements significantly. Results reveal that using hafnium hydride additives at 10 mass% enhanced the heat of combustion of Al+CuO by 12%. The transition of this equilibrium based observation to a non-equilibrium fast heating setup is also investigated using plate deformation tests. Exploding bridge wire heads (EBW) initiated by a capacitive discharge unit (CDU) are used to dent plates and the deformation energies are estimated to observe the effects of varying composites in a non-equilibrium setting. The presence of HfH2 showed improved deformation energies for Al+CuO in the 10%.mass HfH2 range.

Taking polytetrafluoroethylene (PTFE) varying in chain lengths and molecular weight combined with the exothermic surface chemistry of the alumina passivation shell presents results based on very tailorable parameters. Experimentation was performed using simultaneous thermal analysis (STA) that covers both heat flow and mass loss. Flame speeds were also tested and required the use of an altered Bockmon tube method. Results showed a pre-ignition reaction (PIR) with longer chained PTFE samples and not with the shorter chained PTFE samples. The PIR is attributed to fluorine dislodging the hydroxyls from the alumina (Al2O3) surface and forming Al-F structures on the surface of Al2O3. Composites exhibiting the PIR correspondingly result in significantly higher flame speeds. The PIR surface chemistry may contribute to promoting the melt dispersion mechanism (MDM) responsible for propagating energy in nano Al reactions.

LIST OF TABLES

LIST OF FIGURES

CHAPTER 1:

INTRODUCTION

Typically categorized as pyrotechnics, propellants and explosives, energetic materials store chemical energy which is released during a reaction[1, 2]. These materials undergo strong exothermic reactions that arise as a result of interacting reducing and oxidizing constituents, as is the case with thermites or from intermolecular redox processes in purer compounds, as is the case in high explosives[1-4]. The heat produced during these exothermic reactions is due to the internal energy of the products being lower than the internal energy of the reactants. Endothermic reactions would be when the opposite occurs and the products have a higher internal energy than the reactants, which is often characterized by melting [2, 4, 5]. This difference between the internal energies is coined the heat of reaction, where an exothermic reaction would be a heat of combustion and an endothermic reaction would be a heat of melting.

The process and technology used in the making of these energetic materials have remained for the most part unchanged since the black powder invention 220 years BC [1, 6]. Energetic materials are now no longer limited to military needs but also find a use in a wide array of civilian industries like: signal flares, mining, airbags, construction/demolition and fire extinguishing systems[2, 4]. Often times the terms explosives and thermites or pyrotechnics are used interchangeably, but this is incorrect. Explosives are monomolecular and therefore incorporate both fuel and oxidizing parts into one molecule [1, 7-9]. On the contrary, when dealing with thermites and pyrotechnics there has to be a physical mixing of fuel and oxidizer,

unlike the case for organic explosives [1, 10-12]. To illustrate the differences Equation 1 presents an example of a monomolecular nitro glycol explosive.

$$O_2N - O - CH_2 - CH_2 - O - NO_2 \rightarrow 2CO_2 + 2H_2O + N_2 \quad (1)$$

As shown the monomolecular explosive decomposes during its reaction and proceeds to reform into oxidized products. Equation 2 shows the reaction process in a thermite composition.

$$CH_4 + 2O_2 \rightarrow CO_2 + 2H_2O \quad (2)$$

Observed here is that there is a fuel and oxidizer and these 2 reactants react to form the products shown. For a complete reaction it was necessary to have two oxygen molecules for each methane molecule.

A subset of thermites coined Metastable Intermolecular Composites (MIC) represents the composites made up of nanometer range fuels and oxidizers [13, 14]. Aluminum (Al) has quickly become the fuel of choice when working with MICs, due in large to its thin oxide layer that makes it less pyrophoric and more acquiescent to functionalization and pairing with other reactive materials [3, 6, 15, 16]. MICs have drawn so much attention because they present higher energy densities than their organic explosives counterparts [1, 4]. For example the aluminum (Al) and polytetrafluoroethylene (PTFE) thermite reaction produces 21 GJ/m^3 as compared to the best molecular explosive that generates in the range just below 12 GJ/m^3 [17]. Flexibility in the use of MICs allows them to be tailored towards specific goals or desired performance. Some of the parameters usually tailored when working with MICs are: equivalence ratio, particle size, introducing additives or changing the environment within which the reaction takes place [1-4, 12, 18]. These capabilities are

broadened when studying the effects of different ignition methods on the thermite reaction kinetics, where ignition methods are impact, thermal, electric, chemical and mechanical stimuli [12, 19-21].

With the transition into nano-sized fuels and oxidizers, flame speeds exceeding 100 m/s and at times 1000 m/s have been observed when a fluoropolymer or a halogen oxide is reacted with aluminum[22, 23]. Literature reports a unique activation mechanism that encompasses heating, phase changes and rapid pressure build up, coined melt dispersion mechanism (MDM) as it results in a literal dispersion of molten particles[6, 10, 11, 22-25]. This mechanism is documented as being activated with Nano-Al under high heating rate (i.e., $>10^6$ K/s) and high flame speed (i.e., >10 m/s) conditions [10, 11, 25]. When MDM is activated the Al core in a MIC material melts prior to its Al_2O_3 shell breaking and causes a 6% increase in volume[10, 11, 24, 25]. This increase induces heightened pressures of up to 10 GPa in the Al_2O_3 shell which causes fast fracture and spallation of the shell and leads to a pressure gradient that creates an unloading wave dispersing the small Al particles in into the reaction zone where they are then oxidized [6, 10, 24, 25]. The MDM process is composed of multiple steps and is dependent on various conditions simultaneously, with one of the key parameters being the ratio of the shell thickness and particle diameter[6, 10, 11, 24, 25]. This mechanism implies an increase in shell thickness would correlate to an increase in propagation rate [6, 10, 11]. Already critical in the role it plays in the activation of MDM, Al_2O_3 has also been observed to possess a very reactive interface that is documented as bonding with highly electronegative elements like fluorine[9, 26]. When exposed to moisture in air hydroxyls form bonds on the oxide surface and

can be dislodged in the presence of moderate temperatures and elements with stronger affinity. This renders Al_2O_3 a potential proponent for heightened reaction not only due to the effects of its thickness on propagation but also the reactivity of its outer surface.

How tailoring thermites by altering molecular structure, composite additives or using halogen based oxidizers affects their thermal behaviors and reaction kinetics, is assessed in this work. Exploring the feasibility of equilibrium based testing in non-equilibrium settings is also studied. This new knowledge will contribute to improving predictive methods when dealing with these reactive powders and allow for enhanced goal orientated designs.

CHAPTER 2:

OXYGEN SCAVENGING ENHANCES EXOTHERMIC BEHAVIOR OF ALUMINUM FUELED ENERGETIC COMPOSITES

Abstract

The theoretical heat of combustion for aluminum (Al) and copper oxide (CuO) under ideal conditions is roughly 4100 kJ kg^{-1}, but in practice only a fraction of this energy is available for application. Approaching the theoretical value requires innovative strategies for exploiting reaction kinetics. One strategy is to force Al to react CuO as opposed to oxygen from the environment and this approach was shown here to improve the measured heat of combustion significantly. This was achieved through tailoring the mixture using an additive with oxygen affinity prior to Al ignition. The additive is hafnium hydride (HfH_2) and this study examines reaction kinetics for HfH_2 0-60 mass% concentration range using simultaneous thermal-gravimetric analysis (STA). Results reveal that 0-10 mass% HfH_2 additive enhanced the heat of combustion of Al+CuO by 12%. The observed enhancement is attributed to HfH_2 creating oxidation competitions that directly influence the combustion performance of Al+CuO. The transition of this equilibrium based observation to a non-equilibrium fast heating setup is also investigated using plate deformation tests. Exploding bridge wire heads (EBW) initiated by a capacitive discharge unit (CDU) are used to dent plates and the deformation energies are estimated to observe the effects of varying composites in a non-equilibrium setting. The presence of HfH_2 showed improved deformation energies for Al+CuO in the 10%.mass HfH_2 range.

Introduction

Energetic materials that are composites of fuel and oxidizer particles continue to receive considerable attention due to their high energy densities and reaction temperatures. Aluminum (Al) has consistently been the primary fuel in nano-composite metal materials (nano-CMMs) and its combustion has been extensively studied [27-30]. Many oxidizers can be combined with Al but copper oxide (CuO) is a common choice due its high reactivity [31-33]. Also, Al/CuO is noted to have three times the energy density of the monomolecular explosive tri-nitro-toluene (TNT) [34].

The Al+CuO reaction is diffusion controlled such that garnering the full theoretical heat of combustion for this reaction is limited by inherent energy losses. In general, the experimental heats of combustion for Al fueled composite reactions are always sizably below the calculated theoretical values, due to losses and incomplete combustion [35]. Fischer and Grubelich prepared extensive theoretical calculations for hundreds of CMM reactions including data for heats of combustion [36]. While this information is tremendously useful as a gauge for comparing reactions; if reported theoretical heats of combustion could actually be approached, then a plethora of new applications may become available for CMM reactions.

The disparity between theoretical and experimental heats of combustion indicates that a lot of energy is lost through various avenues inherent with diffusion oxidation. Some energy loss may be attributed to the environment and others to physical or chemical limitations. The highly exothermic Al+CuO redox reaction is controlled by the large aluminum oxide (Al_2O_3) heat of formation [37]. An approach to understanding the mechanisms of energy loss involves analyzing the reaction kinetics

with specific focus on characterizing exothermicity as a function of chemistry. This objective will be accomplished using equilibrium diagnostic techniques and will explore the hypothesis that Al may initially oxidize with environmental oxygen prior to the solid oxidizer which may limit the heat of combustion for the solid fuel/oxidizer reaction. In the manufacture of high-vacuum tubes gas has to be removed through a series of heating schedules and then residual gases are extracted using materials called getters[38]. These are chemically active materials such as barium; tantalum and zirconium that combine or react with the gases and as such remove them from the environment[38]. Using the getter idea as a foundation, the following experimental methods were devised and an additive chosen that would perform a similar role to the getters.

Understanding how these equilibrium based results translate to high heating rate initiation is also an objective of this study. A series of experiments were designed using hafnium hydride (HfH_2) additive to Al+CuO. Hafnium possesses various useful properties such as high density (13.31 g cm^{-3}) and large neutron capture cross section such that Hf and HfH_2 are widely used for nuclear reactor and microprocessor applications [39]. The property that renders Hf useful in this work is its affinity for oxygen thus enabling atmospheric oxygen scavenging [40, 41]. This property is shared by H_2 which is also an avid oxygen scavenger [42]. Introducing the HfH_2 acts similarly to the getter setup and provides a way to limit the available atmospheric oxygen in reacting Al+CuO and observe the associated combustion behavior.

Experimental

Materials

Samples used consisted of nano-meter scale Al powder (80 nm average diameter supplied by Nanotechnologies), nano-meter scale CuO powder (50 nm average diameter purchased from Sigma-Aldrich) and micro-meter scale HfH_2 (30 μm average diameter purchased from Goodfellow). All particles have a spherical morphology. The Al+CuO samples were prepared at a stoichiometric equivalence ratio. The specific foundational mixture used is 2Al + 3CuO and HfH_2 is added as a mass percentage as follows: 10%, 20%, 40% and 60%. The respective quantities of powders are measured out and suspended in a hexane solution. This solution is then placed in a Misonix S3000 sonicator and sonicated for duration of 1 min. This sonication program is run cyclically at 10 s on 10 s off, to avoid damaging the oxide shell during this intimate mixing process and allowing for cooling periods. Post sonication the mixture is poured into a Pyrex dish and the hexane evaporates in a fume hood and the mixed powder is reclaimed for further experimentation.

Thermal Analysis

A Netzsch STA 409 (DSC/TGA) differential scanning calorimeter and thermogravimetric analyzer was used for the thermal analysis of the samples. Temperature calibrations for the instrument were performed using melting of a set of metal standards resulting in a temperature accuracy of ±1 ^{o}C. Platinum crucibles with alumina liners were used and contained 5 mg of sample during testing. The samples were programmed to be heated from 30-1000 ^{o}C at a rate of 10 ^{o}C min^{-1}. Tests were performed in both air (i.e., oxygen/argon environment: 20/60 mL min^{-1}) and argon

environment. When running tests in an argon environment, the DSC column was evacuated to 1 x 10^{-4} atmospheres using a Pfeiffer model TMU turbo pump and then backfilled and purged with argon at a flow rate of 70 mL min^{-1} for the remainder of the cycle. Sintering can occur during heating and melting, ultimately affecting heat transfer in the DSC measuring head. To insure consistency, repeatability and minimize artifact alterations of results, three experiments were performed for each sample.

Energy Deformation Tests

A capacitive discharge unit (CDU) (Cal Av Labs, Inc.) was used to produce the energy to detonate the EBW (RP-8X, Teledyne Risi). Initiation energies are controlled by an adjustable capacitor bank of 1-7μF and input voltages of 1.2 to 5.5 kV. When triggered, the gas in its spark gap is ionized and creates conductive plasma allowing current flow to the EBW. The EBW is a type of detonator which utilizes shockwaves to initiate reaction. Figure 1 shows the EBW is positioned such that the copper plate absorbs the full blast of the reaction.

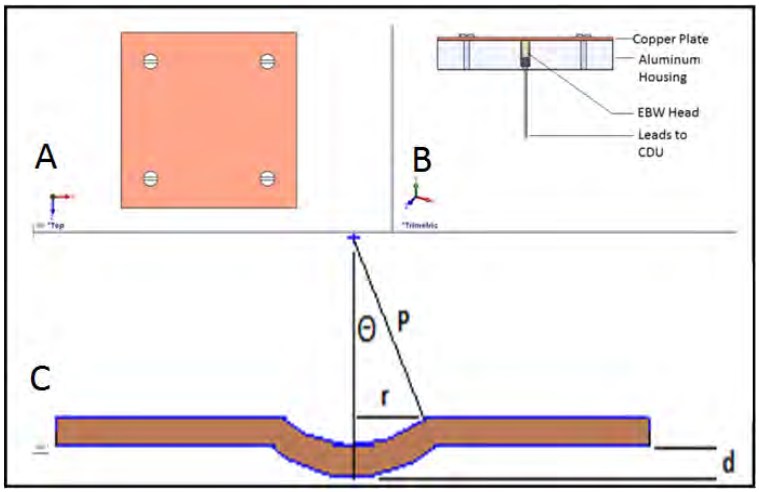

Figure 1: EBW Housing Test Setup A. Top view B. Side view C. Post detonation dent

The head is filled with the sample and the shock wave that initiates reaction is due to the bridge wire explosion upon receiving the high input from the CDU. The amount of the powder that filled the head was approximately 70 mg for each test run. The reaction in the EBW head produces a dent in the copper plate which is used to estimate the deformation energy. This measurement provides an indication of the energy responsible for deformation. The following analysis is used to quantify this value from the plate dent.

The analysis assumes work hardening is ignored which renders the yield strength constant and simplifies the calculations. From the dimensions shown in Fig. 1, $(P-d)^2 + r^2 = P^2$ and $P = \frac{r^2+d^2}{2d}$. The angle is determined as $\Theta = \sin^{-1}\frac{r}{p}$. The original length of the curve in Fig. 1 just prior to deformation is $L_0 = 2r$ such that the curved length is $L_1 = 2P\Theta$. The uni-directional strain can therefore be calculated as $\varepsilon = \frac{L_1 - L_0}{L_0}$ and the bi-directional is $\varepsilon_{eff} = 2\,\varepsilon = \frac{2P\Theta - 2r}{2r}$. Now a work per volume can be calculated. In this case, plastic work per volume is $\frac{P_w}{V} = Y\varepsilon_{eff} = 2Y\frac{(P\Theta - r)}{r}$, where Y is the yield strength of the plate. The volume of the dent is $V = \pi r^2 t$, where t is the copper plate thickness (and assumed constant). Therefore energy causing the deformation $\mathrm{Q} = \frac{P_w}{V} * V = 2\pi r t * Y * (P\Theta - r)$. All experiments were performed with HfH_2 additives ranging 0-60 mass% to the base formulation Al + CuO. The resulting deformations were analyzed and measured using image-J software package. Deformation dimensions were acquired and energy calculations were performed following the analysis described above.

Results

Figure 2A shows the exotherm of the Al+CuO reaction is increased with the addition of 10% HfH_2 and then proceeds to decrease sizably with continual increase in HfH_2 concentration. A similar pattern is observed in the thermal gravimetric analysis of the different mixtures (Fig.2B). A greater mass gain is observed with 10% HfH_2 addition and then a gradual decrease is observed with increasing HfH_2 concentration.

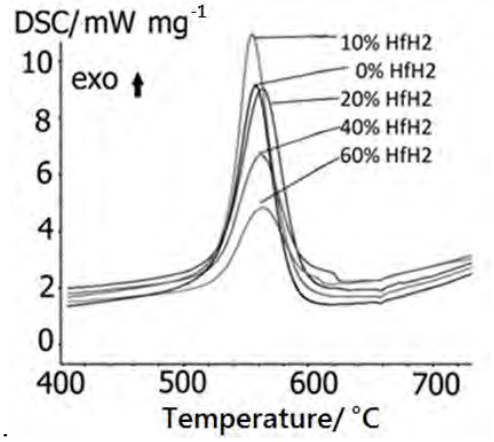

.

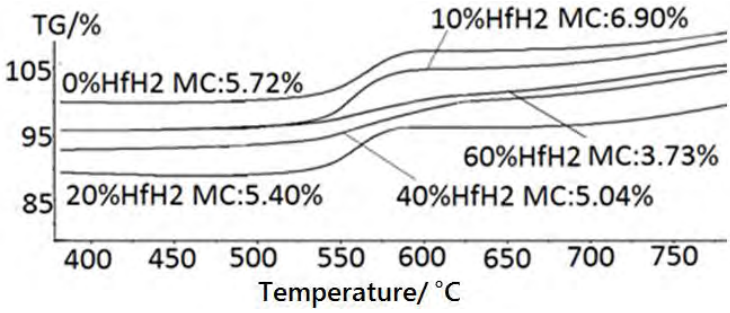

B.

Figure 2:A. Heat flow as a function of temperature (from DSC); and, B. Mass gain as a function of temperature (from TG) for respective mixtures.

The energy released upon combustion was estimated by calculation of the area under the exothermic peaks in Fig. 2A. The area calculations were performed for the following: Al+CuO (in air), Al+CuO (in argon) and Al+CuO+HfH_2 10% (in air) using the Proteus thermal analysis software. The results are presented in Table 1 as the heat of combustion (ΔHc). A theoretical value was also calculated for Al+CuO using

thermodynamics software package REAL. In fact, the REAL code analysis for heat of combustion was performed for a wide range of stoichiometry and the optimum heat of combustion is obtained at equivalence ratio (ER) equal to 1.0.

Table 1. Theoretical and experimental heat of combustion

Mixture	ΔHc/ J g^{-1}
Al+CuO(theoretical)	**4100**
Al+CuO(in argon)	**2087**
Al+CuO(in air)	**1700**
Al+CuO+HfH2 10%(in air)	**1900**

Figure 3 shows the deformation energy as a function of HfH_2 mass% added to Al + CuO. The 0 mass% HfH_2 deformation energy is 25J but for 10% HfH_2 additive it increases to 45 J.

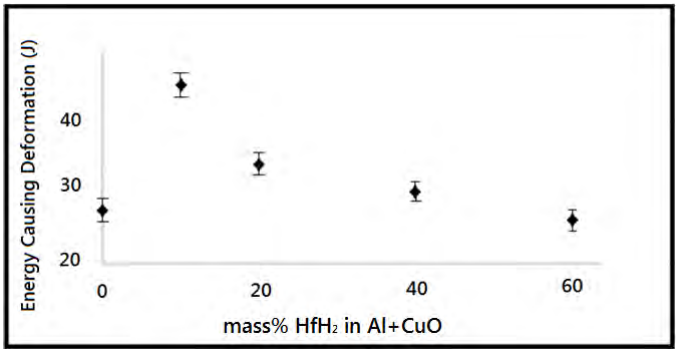

Figure 3: Deformation energy as a function of mass% HfH2 in Al+CuO

The theoretical value for Al+CuO assuming the same amount of powder is 281 J. In comparison to the equilibrium based testing, the increase in energy available from the Al+CuO+10mass% HfH_2 is 8% and in good agreement with the 12% observed in the equilibrium case (i.e. Figs 2A and 3). As the concentration of HfH_2 additive

increased the deformation energy decreased; and, this observation is consistent with the results in Fig. 2A.

Analysis

To understand the reaction kinetics associated with the addition of HfH_2, several additional experiments were performed. First, DSC and TG tests were performed in air on individual powders of Al, CuO and HfH_2. Further testing examined thermal behaviors of Al+CuO in both air and argon environment.

The first TG experiment observed the de-hydrogenation and oxidation of Hafnium (Hf) as shown in Fig. 4. HfH_2 decomposition is documented to dissociate H_2 at 300 °C, followed by oxidation of both Hf and H_2 [43]. This H_2 loss is not easily spotted in Fig. 4 because the mass of H_2 is miniscule in comparison to the mass of HfH_2 (H is 1.01 AMU while Hf is 178.49 AMU). Figure 4 shows an initial mass loss attributed to dissociating H_2 and increasing mass gains attributed to oxidation of Hf.

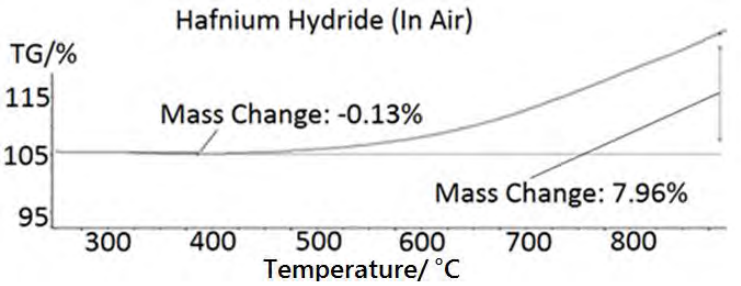

Figure 4: Hafnium hydride in an air environment with decomposition and oxidation represented as mass loss and gain from TG analysis at a heating rate of 10 °C min-1.

The oxidation of Hf is documented as going from Hf to HfO to HfO_2 [44]. Taking this into consideration, if HfH_2 lost H_2 and gained oxygen to form HfO, it would have an approximate 8% increase in mass. This is observed at 900 °C in Fig. 4.

Figure 5 examined the reduction process of CuO using TG. Pike et al. [45] observed and presented CuO reduction kinetics as follows: CuO → Cu2O → Cu.

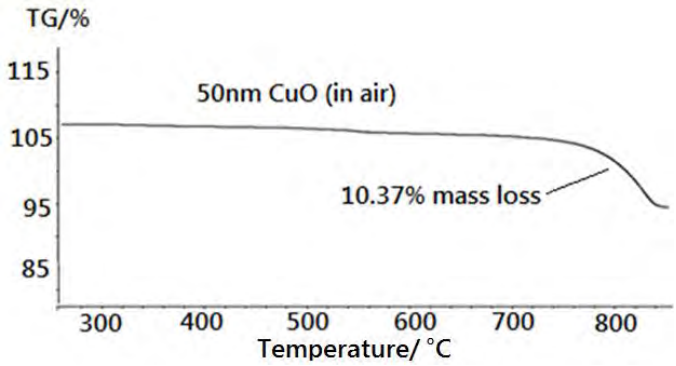

Figure 5: Copper oxide reduction seen as mass loss from TG analysis in air at 10 oC min-1.

In Fig. 5 the mass remains constant until 800 °C then begins a sizable mass loss, measured as 10.37%. When CuO is reduced to Cu_2O, half the oxygen from CuO is lost [45]. Mass of CuO from periodic table additions is 79.54 AMU. The percent of oxygen in this mix is calculated to be approximately 20%, therefore losing half the oxygen would equate to a 10% loss which is observed in Fig. 5 and this mass change is therefore attributed to the reduction of CuO to Cu_2O.

Further DSC and TG analyses were performed on HfH_2+CuO and Fig.6 shows that no exotherm is observed and the slight mass gain occurs at high temperatures (i.e., > 600°C) and exceeding the dissociation temperature of HfH_2.

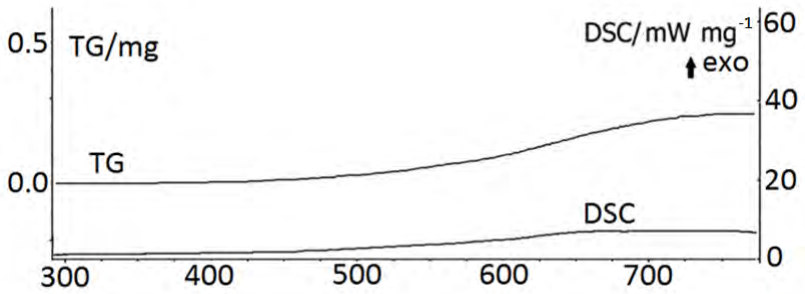

Figure 6: Heat flow (DSC) and mass change (TG) for HfH2+CuO in argon at °C min-1.

These results confirm that HfH_2 will favor reaction with atmospheric oxygen and its interactions with CuO are negligible.

Aluminum oxidation in an air environment at a heating rate of 10°C min^{-1} is shown in Fig. 7. Both the TG and DSC results agree with the literature[28] and show oxidation beginning at 540 °C but no exothermic peak is manifest.

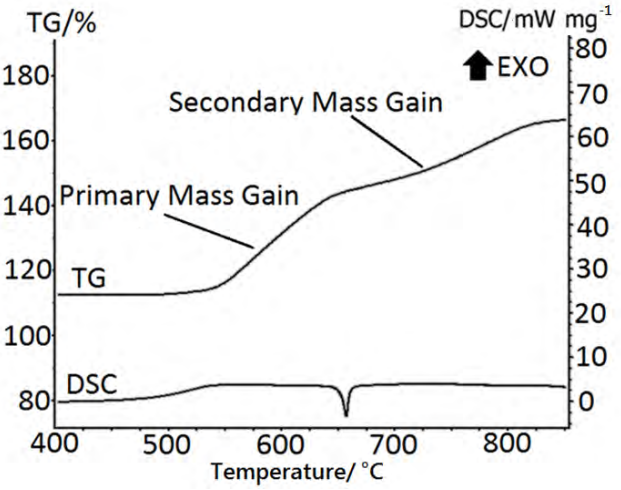

Figure 7: Heat flow (DSC) and mass loss (TG) for 80nm average diameter aluminum powder in air at 10 °C min-1.

Therefore the exotherms observed in Fig. 2A are due to Al reacting with oxygen from CuO. In agreement with the observations of Trunov et al. [46], oxidation begins at much lower temperatures than the onset of Al melting (660 °C). The primary

and secondary mass gains are attributed to phase changes within the material [27, 28]. In fact, five processes have been associated with Al oxidation that may account for the mass gains shown in Fig. 7: (1) amorphous oxide growth, (2) phase change from amorphous to γ-alumina, (3) γ -alumina growth, (4) phase change from γ to α-alumina, and (5) α -alumina growth [46, 47].

All the above observations suggest the effect of oxygen in air differs from the effect of oxygen in CuO in relation to the results shown in Fig. 2. To confirm this, DSC and TG tests with Al+CuO were performed in air and an argon environment. Figure 8A shows a mass gain in air but not argon. In both cases there was an exothermic reaction, as indicated in Fig. 8B.

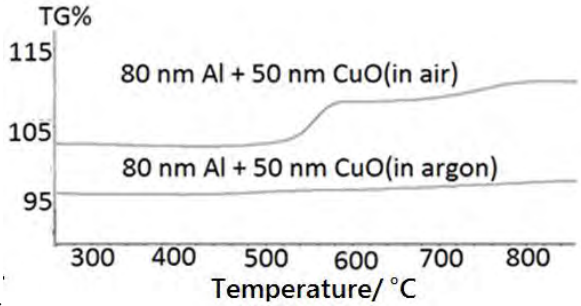

A.

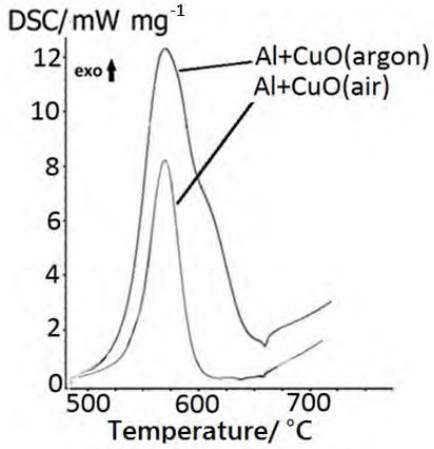

B.

Figure 8: A. Mass change (TG); and, B. Heat flow (DSC) for Al + CuO in both air and argon environments at 10 ^{o}C min^{-1}heat rate.

The mass gain is a result of the oxygen in the air, in comparison to no gain in the argon, indicating reaction between the solid reactants only. Furthermore Fig. 8B shows that the onset of reaction is the same in argon as air, which would indicate the reduction of the oxidizer as the rate determining step in the reaction. This is important because it cancels out any possibility that the exotherm may be due to oxygen in the environment. Erickson et al. experimented with Al+CuO in air and confirmed the mass gain in Fig. 8A, which initiates at temperatures almost 100ºC lower than Al melting temperature [48]. The increase in mass corresponds with the exotherm onset at 530ºC. The behavior correlates well with results in Fig. 7 which show Al oxidation onset at 530ºC. This confirms that reaction is based on oxidizer reduction and not influenced by atmospheric oxygen.

Discussion

Equilibrium Study

Figures 2 and 4-8 indicate an oxidation-reduction competition is created by the presence of HfH_2 and impacts the reaction behavior. When Al+CuO is tested in air with no HfH_2 additive, Al is potentially oxidized through two avenues. The first involves easily accessible oxygen from air that requires less energy than the second avenue of oxidation through the oxygen from the solid oxidizer. When HfH_2 is present, things change a little. Looking at the heats of formation for the oxidation of HfO, H_2O and Al_2O_3 presented in Table 2, H_2O would initiate prior to HfO which would in turn initiate prior to Al_2O_3 [30, 44]. Also, the electronegativity of the individual elements are as follows O > H > Al > Hf.

Table 2. Heats of formation for oxidation products [30, 44]

Material	Heat of Formation/ KJ mol^{-1}
HfO	**-564.80**
HfO_2	**-1144.74**
H_2O (gas)	**-241.82**
Al_2O_3	**-1669.80**

The following mechanism explains the enhanced exothermic behavior observed for 10% HfH_2 additive. For the 10%HfH_2 mixture the first thermal effect observed is Hf dissociating from H_2 around 300^{o}C and reacting with oxygen in air followed by Hf oxidation around 450-460^{o}C (Fig. 4). This forces Al, once it begins oxidation around 540^{o}C, to acquire its oxygen solely from the solid oxidizer, thereby producing improved combustion based on a thorough reduction of the solid oxidizer. Essentially, Hf and H_2 consume oxygen from the air thereby promoting Al oxidation with oxygen from CuO.

With the increase in HfH_2, there is an increase of both H_2 and Hf that will both scavenge for oxygen. Bond et al., studied the kinetics of copper oxide reduction using H_2, confirming the reaction $CuO(s) + H_2(g) \rightarrow Cu(s) + H_2O(g)$, by approximations using a semi-empirical formula[42]. While not directly observed in Fig. 6, H_2 reducing CuO may also promote enhanced combustion. The electro-negativity of H and the low heat of formation of H_2O also lend to this argument.

Therefore with the increased concentration of Hf and H_2 promoting oxidation and the lower heats of formation of HfO and H_2O (g), more energy is facilitating the

formation of hafnium oxide and water vapor. Subsequently less energy and oxygen are available for the formation of alumina. Therefore there appears to be a region where mathematically there is an optimal balance of HfH_2 scavenging the oxygen in the air, allowing maximized access of Al to the oxidizer, CuO.

It is observed in Fig. 4 that Hf only reaches a stable HfO chemistry at 900°C. Yet it continues to oxidize as long as oxygen is available, as it proceeds from HfO to HfO_2 [44]. The Al on the other hand oxidizes to Al_2O_3 and then proceeds to go through various phase changes [28]. The temperature range in which it further oxidizes to Al_3O_4 (i.e., 1500°C and higher) is not reached and so the secondary mass gain in Fig. 2b is attributed to the stabilizing of Al_2O_3 and the continued oxidizing of Hf as the CuO reduces to Cu_2O [28, 45, 47].

Table 1 provides two points of interest. First, Table 1 confirms that ΔHc of Al+CuO+HfH_2 is closer to Al+CuO in an argon environment rather than air, which is expected since Al with the HfH_2 additive will oxidize from the solid oxidizer and not oxygen in the air. Second, there is a sizeable improvement in ΔHc for Al+CuO+HfH_2 in comparison to Al+CuO. The disparity between Al+CuO+HfH_2 and the result from the argon environment indicates that the concentration of HfH_2 may still be tailored to further improve ΔHc and that this range would be found around the 10% HfH_2 additive. This was not pursued experimentally due to the high density of the Hf that made weighing concentrations as small as utilized in the DSC virtually unfeasible.

The Al+CuO+10%HfH_2 mixture could be considered fuel rich because Al+CuO is prepared stoichiometric. Recalculating the equivalence ratio (ER)

considering HfH_2 as a fuel results in Al+CuO+10% HfH_2 with an ER = 1.2 (i.e., slightly fuel rich). As a comparison, Fig. 9 shows the exothermic behavior of three samples, two with ER = 1.2 (i.e., Al+CuO and Al+CuO+10%HfH_2) compared with the stoichiometric mixture of Al+CuO.

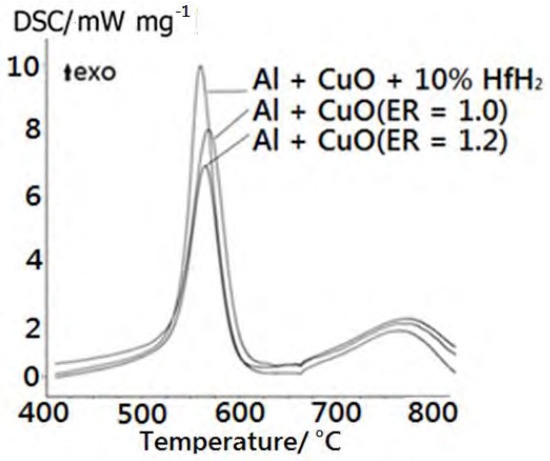

A.

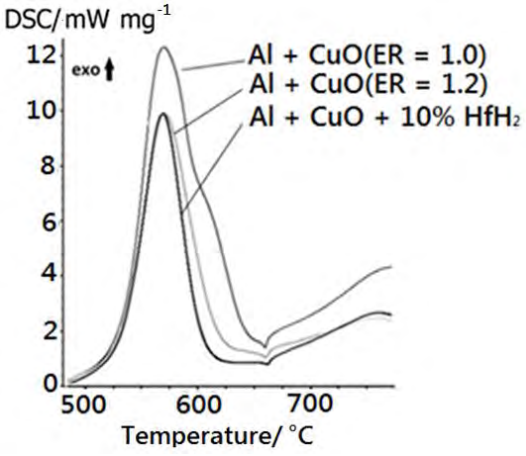

B.

Figure 9: A. Heat flow as a function of temperature examined at 10 $^oC\ min^{-1}$in an air environment; and, B. in an argon environment for respective mixtures.

Figure 9A shows that in air Al+CuO+10% HfH_2 has a greater exotherm than Al+CuO (ER = 1.0) which has a greater exotherm than Al+CuO (ER = 1.2). The lack of coherence between the Al+CuO (ER = 1.2) and Al+CuO+10%HfH_2 indicates that HfH_2 is not acting like fuel in the same way as Al. These results are consistent with REAL code analysis that found equivalence ratio 1.0 to be most favorable.

The same mixtures observed in Fig. 9A were then examined in an argon environment. Figure 9B shows that without air, the improvements in combustion seen with the Al+CuO+10%HfH_2 are negated, due to lack of atmospheric oxygen. In this case, the HfH_2 may be competing with Al for oxidation with CuO such that the two fuel rich stoichiometry behave similarly.

Theoretical calculations were performed using thermodynamic equilibrium software, REAL to confirm the experimental results. Two quantitative outputs were produced, one simulating an argon (i.e., oxygen free) environment and the other an oxygen environment. The results are shown in Fig. 10A and 10B. The results closely follow the trends observed experimentally indicating balances for HfH_2 additions coupled with environmental oxygen concentration for optimization of the Al+CuO reaction.

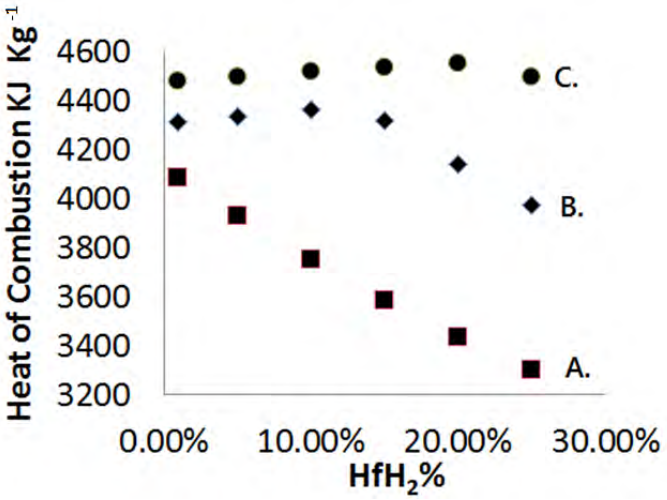

Figure 10: Theoretical calculations for heat of combustion for: A. Oxygen free (i.e., argon simulation); B. Oxygen; and, C. Excessive oxygen environment.

As environmental oxygen concentration increases, more hafnium hydride additive is necessary to achieve improved heat of combustion. This is shown in Fig.

10C with a case of increased environmental oxygen. It is observed that the ideal amount of HfH_2 has increased to 20%. This will be the case if the amount of Al+CuO remains constant.

Equilibrium Study Extended to Al+WO_2

With interest to confirm more universal validity of the influence of HfH_2, similar experiments were performed with a different oxidizer, tungsten dioxide (WO_2) and a mixture composed of Al +WO_2 with varying concentrations of HfH_2. Figure 11 shows the results and two points are apparent. First, the behavior observed with CuO is mimicked with WO_2; and, second the amount of increase in the exotherm sizably increased in comparison to Al+CuO.

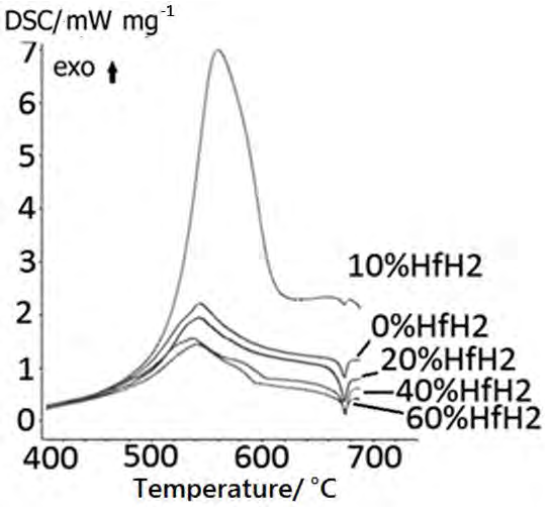

Figure 11: Heat flow (DSC) curves for Al+WO_2 performed in air at 10 ^{o}C min^{-1}.

This interesting observation provokes additional questions about which mixtures would exhibit the greatest exothermic effects based on the presence of the HfH_2 that could be explored further in future work.

Detonation Initiation

The method of sample encapsulation prior to combustion limited access to environmental oxygen in the EBW head and enabled the reaction kinetics observed in equilibrium testing to be replicated in these high heating rate tests. The increased deformation energy in Fig. 3 may be correlated to the results in the equilibrium tests that showed increased heats of combustion for 10mass% HfH_2 additive. A low dissociation temperature for HfH_2 promotes Hf and H_2 reaction with atmospheric air prior to Al ignition and prior to CuO decomposition. This additive scavenges atmospheric oxygen and promotes more favorable reaction kinetics between Al and CuO which in turn increases the chemical energy available from the reaction. This is observed in the larger plate deformation and higher deformation energy associated with 10mass% HfH_2 additive. Excess HfH_2 (i.e., > 10 mass%) diminishes the balance for the oxygen environment within the EBW head and leads to competing oxidation pathways for all the fuels that decrease the overall energy available. Therefore the presence of the HfH_2 appears to maintain its oxygen scavenging characteristics in the confines of the EBW head such that the non-equilibrium results behave similarly to the equilibrium results. These results have impact on ballistic applications where thermite powders are used as primers in confined environments. Specifically, tailoring the composite with an oxygen scavenging additive may promote increased chemical energy potential.

Conclusion

Aluminum (Al) fueled reactions show improved combustion efficiency when environmental oxygen is minimized, and Al reaction with the solid oxidizer is

encouraged. Introducing an oxygen scavenging additive, hafnium hydride (HfH_2), into the reaction creates oxidation competitions that improve combustion. Specifically, HfH_2 reacts with atmospheric oxygen just prior to Al ignition such that improved heat of combustion up to 12% was achieved with 10% HfH_2 addition. Beyond 10%, HfH_2 competes with Al for reaction with the solid oxidizer producing diminished heats of combustion. Improved combustion behavior is indeed feasible and limiting the oxygen available for reaction to that contained in the solid oxidizer has been observed to be a successful method of achieving greater overall heat of combustion. When observing detonation initiation, HfH_2 was shown to significantly increase the energy available from the Al+ CuO composite in detonation ignition tests. The improvement is attributed to reaction kinetics that forces Al to react with CuO instead of oxygen from the environment. These results have impact on ballistic applications where thermite powders are used as primers in confined environments. Specifically, tailoring the composite with an oxygen scavenging additive may promote increased chemical energy potential.

CHAPTER 3:

EXOTHERMIC SURFACE CHEMISTRY ON ALUMINUM PARTICLES PROMOTING THE MELT DISPERSION MECHANISM

Abstract

The unique exothermic surface chemistry associated with the alumina passivation shell surrounding aluminum (Al) particles and fluorine from fluoropolymer materials is investigated. In particular, polytetrafluoroethylene (PTFE) has been synthesized with varying chain lengths and molecular weights and combined

with nanometric Al fuel particles. The Al-PTFE samples were analyzed using equilibrium diagnostics including differential scanning calorimetry (DSC) and thermogravimetric analysis (TGA) as well as non-equilibrium combustion characterizations such as flame speed measurements. The objective was to understand the effects of varying PTFE microstructures on the kinetic and energy propagation behaviors of these composites. Results showed a pre-ignition reaction (PIR) with longer chained PTFE samples and not with the shorter chained PTFE samples. The PIR is attributed to fluorine dislodging the hydroxyls from the alumina (Al_2O_3) surface and forming Al-F structures on the surface of Al_2O_3. Composites exhibiting the PIR correspondingly result in significantly higher flame speeds. The PIR surface chemistry may contribute to promoting the melt dispersion mechanism (MDM) responsible for propagating energy in nano Al reactions. Composites with a PIR also have higher heats of combustion in both the PIR and main reaction exotherm. These results help elucidate the influence of molecular scale surface chemistry on macroscopic energy propagation.

Introduction

Composite energetic materials that include aluminum as the fuel and a fluoropolymer as the oxidizer have recently received more attention in the research community [6, 49-52]. One composite of particular interest is aluminum (Al) and polytetrafluoroethylene (PTFE). These mixtures introduce a new way of thinking about aluminum reactivity because the fluorine is the primary oxidizer reacting with aluminum, as opposed to oxygen based solid oxidizers[6, 50-52]. The Al/PTFE

reaction produces 21 GJ/m^3 as compared to the best molecular explosive that generates in the range just below 12 GJ/m^3 [17].

Flame speeds exceeding 100 m/s and at times 1000 m/s are observed when nano-Al fuel particles react with a halogen oxide, or fluoropolymer [22, 23, 53]. Aluminum particles are passivated with a 2-4 nm thick alumina shell that is independent of particle size [5]. As the Al particle size is reduced, the specific surface area of the particles increases dramatically such that a larger concentration of the overall powder is alumina. Because alumina has high insulating characteristics, one may predict that the larger concentration of alumina may act to retard energy propagation. However, the presence of the alumina shell plays a critical role in promoting heightened levels of reactivity for nano-Al particles through activation of a unique reaction mechanism coined, the melt dispersion mechanism (MDM) [6, 10, 22-25, 53, 54]. Literature reports the melt dispersion mechanism (MDM) as the operating mechanism for nano-Al reactions under high flame speeds (i.e., >10 m/s) and high heating rate (i.e., > 10^6 K/s) conditions [6, 10, 11, 25]. The MDM is explained as a multi-step process beginning with the melting of the Al core that causes a 6% increase in volume within the core of the particle. This volumetric expansion is accompanied with heightened pressures in the Al core up to 1-3 GPa and tensile hoop stress in the oxide shell of up to 10 GPa. This hoop stress causes fast fracture and spallation of the shell. The exposed molten Al surface leads to a pressure gradient that creates an unloading wave dispersing small Al droplets in all directions [6, 24, 25]. The dispersion of aerosolized molten Al droplets are quickly oxidized and therefore the reaction is limited to oxidation by diffusion through the alumina shell and result in

extremely high reaction rates [6, 10, 25]. The MDM had been confirmed for fast oxidation of Al nano-particles with oxygen based oxidizers [6, 10, 22, 25] but also for fluorination reactions [6]. Specifically, Watson et al. [3] examined Al combined with polytetrafluoroethylene (PTFE) and found flame speeds of up to 827 m/s such that MDM is activated by fluorination.

The objective of this study is to examine the reactivity of Al + PTFE as a function of PTFE chain length and molecular weight. Specifically, this study focuses on how the polymeric molecular structures of PTFE influence reaction kinetics as well as energy propagation when combined with Al particles. Simultaneous Thermal Analysis (STA) is performed to observe heat flow and mass loss behaviors at the early stages of PTFE decomposition and Al reaction. Flame speed experiments were also performed to link the reaction kinetics to a macroscopic energy propagation mechanism. Analysis of the results shows how molecular level surface chemistry promotes the melt dispersion reaction mechanism for nano-Al particle combustion.

Experimental

Sample preparation

The 80nm average diameter aluminum (Al) particles were supplied from Novacentrix and used as the fuel particles in the composite mixture. Alumina (Al_2O_3) encapsulates the Al core with a layer 4 nm thick, passivating the fuel from spontaneous reaction with surrounding oxygen. Polytetrafluoroethylene (PTFE) was used as the oxidizer and supplied by DuPont. Five PTFE samples varying in molecular structure were studied each varying in degree of polymerization (*DP*) calculated as shown in Eq. (1).

$$DP = MWm/MWu \quad (1)$$

In Eq. (1) MWm is the molecular weight of the macromolecule and MWu is the molecular weight of the structural unit. Therefore, the chain lengths from smallest to largest are DuPont Zonyl®: PTFE MP1100 < PTFE MP1600 < PTFE MP1400 < PTFE MP1200 < PTFE MP1000.

To simplify recognition Table 3 presents physical properties of the powders and nomenclature for referring to the composites used in order of increasing chain length.

Table 3: The PTFE particle properties and associated nomenclature.

Name	Abbreviated Name	Composite	Avg PTFE Bulk Density (g/L)	Particle Diameter (microns)
PTFE MP1100	P1	Al/P1	300	4
PTFEM P1600	P2	Al/P2	350	12
PTFE MP1400	P3	Al/P3	425	10
PTFE MP1200	P4	Al/P4	450	3
PTFE MP1000	P5	Al/P5	500	12

All composites were prepared at a 70/30 fuel/oxidizer mass ratio. This fuel rich mixture was selected as a safety precaution to protect the thermal kinetics equipment from violent reactions usually experienced in mixtures with more than 30 wt.% PTFE under slow heating parameters [52]. The mixtures were balanced according to Eq. (2) and a 6.5 equivalence ratio.

$$3C_2F_4 + 4Al \rightarrow 4AlF_3 + 6C_{graphite} \quad (2)$$

The respective quantities of powders are suspended in a hexane solution and placed in a Misonix S3000 sonicator and sonicated for 1 min duration. This sonication program

operates cyclically at 10 s on and 10 s off, to avoid damaging the oxide shell during mixing. Post sonication the mixture is poured into a Pyrex dish such that the hexane evaporates in a fume hood and the mixed powder is reclaimed.

Reaction kinetics

Simultaneous Thermal Analysis (STA) was performed using a Netzsch STA 409 differential scanning calorimeter and thermogravimetric analysis (DSC/TGA). The system is programed to heat the samples at a rate of 25 ^{o}C/min from room temperature to 800 ^{o}C. Approximately 3 mg samples were loaded into platinum crucibles and placed into the STA. Tests were performed in an argon environment; the STA column was evacuated to 1 x 10^{-4} atmospheres using a Pfeiffer model TMU turbo pump and then backfilled and purged with argon at a flow rate of 70 mL min^{-1} for the remainder of the cycle. Sintering can occur during heating and melting, ultimately affecting heat transfer in the STA measuring head. To insure consistency, repeatability and minimize artifact alterations of results, three experiments were performed for each sample. Temperature calibrations for the instrument were performed using melting of a set of metal standards resulting in a temperature accuracy of ±1 ^{o}C.

Integrating the area under the DSC exotherm, above the base line, provides the total enthalpy change or heat of combustion (*H*) for the process in accordance with Eq.3.

$$\int \left(\frac{dH}{dt}\right)_{sample} dt = \Delta H_{sample} \qquad (3)$$

The rate of mass loss (e.g., rate of gas generation) was estimated for each test. The process followed analyzed the slope of the mass loss curves at the onset of phase change, where the slopes represent the rate of mass loss per degree.

Flame Speed Test

Figure 12 presents a schematic of the setup. These experiments were performed in a closed configuration using a flame tube bench mark diagnostic detailed in [7], and summarized here. The closed configuration used tubes with dimensions of inner and outer diameter 3 and 8 mm, respectively, and length of 10 cm. The tube is filled with 500 mg of powder and placed on the vortex to reduce voids and minimize density gradients. Ignition is via nichrome wire secured at one end of the tube or notch and heated at 10 V by a variac transformer. The tube is placed in a metal casing with a viewing window that allows data collection using a high speed camera. A Vision Research Phantom v 7.1 high speed camera with a Nikon AF Nikkor 52mm 1:2:8 lens, captures the images examined in the flame speed analysis. The camera was set to 160,000 frames per second (fps) for image collection. Given a time and length scale dependent on sample rate of recording, the flame front displacement is tracked by the software and recorded for velocity calculation purposes.

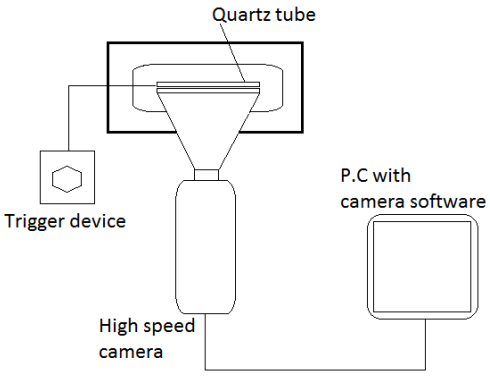

Figure 12: Flame velocity experimental setup.

Results

Reaction Kinetics

Figure 13 shows the heat flow results from DSC analysis and mass loss results from TG analysis for the different composites. The three longer chains show a smaller exotherm prior to the larger one, which is not the case for the two shorter chain length polymers. Starting at Al/P3, increasing the chain length causes a delay in the onset temperature of the smaller exotherm while the larger remains constant. Table 4 presents the data from Fig.13.

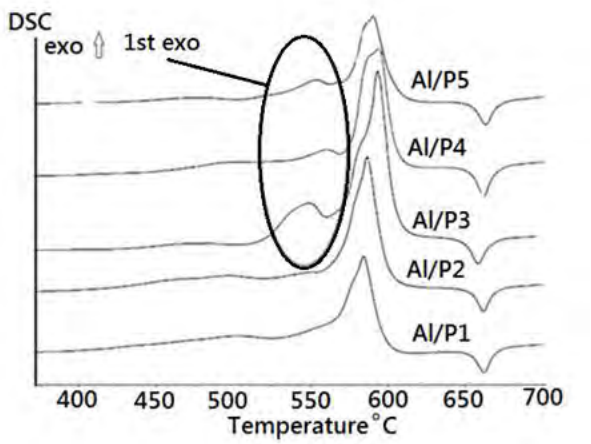

Figure 13: Graph showing heat flow as a function of temperature for each composite, with exotherm in the positive y-direction.

Table 4: Tabulated summary of mass loss and onset temperatures for mass loss or 1st exotherm and heats of combustion for 1st and 2nd exotherm, with NA representing not applicable.

Composite	Mass loss at 1st exotherm	Mass loss onset	Onset of 1st exotherm	Onset of 2nd exotherm	ΔH of 1st exotherm	ΔH of 2nd exotherm
Al/P5	0%	NA	542.8 °C	567.1 °C	33.5 mJ/mg	702.3 mJ/mg
Al/P4	0%	NA	532.2 °C	564.4 °C	34.9 mJ/mg	1028 mJ/mg
Al/P3	0%	NA	524.1 °C	565.2 °C	216.2 mJ/mg	1331 mJ/mg
Al/P2	1.22%	501 °C	NA	566.4 °C	NA	838.3 mJ/mg
Al/P1	1.32%	466 °C	NA	565.6 °C	NA	819 mJ/mg

These results show the two samples that did not exhibit a smaller exotherm have an initial mass loss that the others do not. Even though there are variations in the onset of the 1st exotherm, there is a consistency about the 2nd exotherm for all samples. Heats of combustion for the 1st exotherm increase as the chain shortens, while the heats of combustion for the 2nd exotherm show a peak at Al/P3 and then decreases with both increase and decrease in chain length from that pinnacle.

For comparison purposes the PTFE samples were tested alone in the STA at the same settings as the composites. No exotherms were exhibited but an endotherm indicative of the polymer's degradation was present. The extracted mass loss results are plotted against the Al/PTFE results and presented in Fig.14.

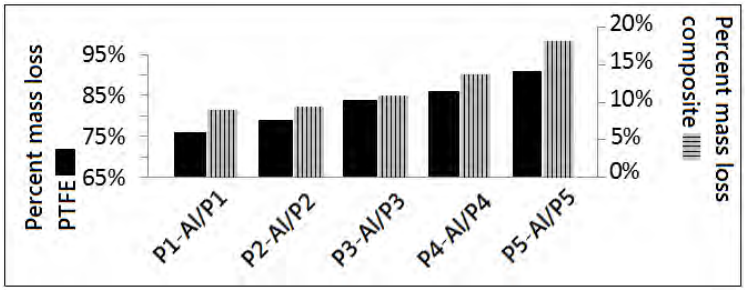

Figure 14: Mass loss trends for PTFE samples; legend indicated alongside axis label.

Similar to the composite mixtures, the PTFE samples maintain a linear behavior in mass loss with the shorter chains exhibiting lower in both categories. These results also show substantially greater mass loss in the case of the PTFE alone in comparison to the composite samples (i.e., approx. 75% compared with 10%, respectively). In both cases the longer chains show greater mass loss in comparison to the shorter chains.

The mass loss rates were calculated and the results are presented in Table 5. The values are fairly consistent in each case and no pattern is observed.

Table 5: Average rate of mass loss calculated for each composite.

Name	Ave Rate of mass loss (% /s)
Al/P1	0.38
Al/P2	0.34
Al/P3	0.36
Al/P4	0.4
Al/P5	0.36

Flame Speed

Results from the flame speed measurements are presented in Fig.15. Three experiments were performed for each sample to evaluate the repeatability of the measurement which is found to be the largest source of uncertainty. The uncertainty in these measurements is determined to be $\pm$4.08 m/s. It is noted that the equivalence ratio was selected to compare with the equilibrium STA testing, yet the measurements are still compatible to Watson et al.[53] for similar fuel rich ratios.

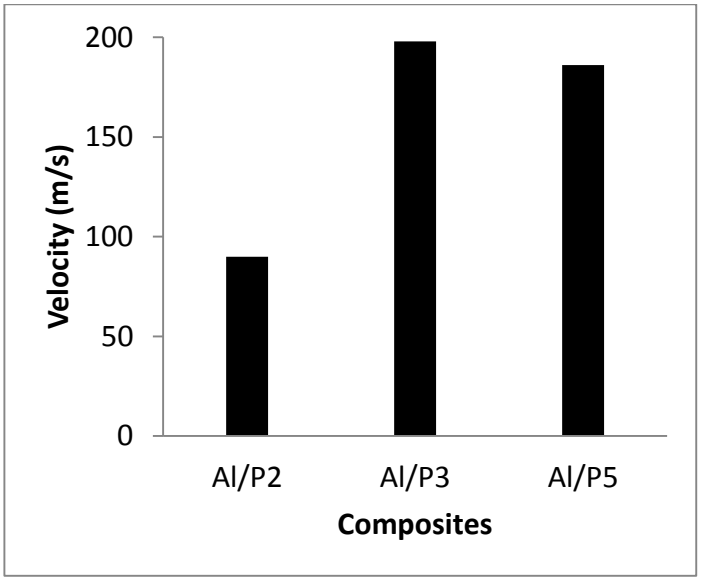

Figure 15: Flame speed results for each composite (max 198 m/s).

Discussions

From polymer chemistry it is known that longer chains exhibit entanglements and reduced mobility; they also have increased density (Table 3) as compared to shorter chains [55, 56]. Longer chains dissociate faster in comparison to shorter chains because they are less stable and form radicals more readily [56]. In this study the initial differences between longer and shorter chains are found in the STA results shown in Fig.13 and Table 4. The longer chains have greater mass loss than the shorter chains and this is also observed in the solo polymer results shown in Fig.14.

The heat flow (i.e., DSC) results show a common exotherm in all experiments just below 600°C. Also exhibited is a smaller initial exotherm in the longer chained polymer composites and none in the shorter chained composites. Since Al_2O_3 degradation temperature is not yet reached at 540 °C when this smaller exotherm is initiated, it is assumed that this initial exotherm results from reaction involving Al_2O_3 and C_2F_4. This corroborates well with Sarbak et al. [26] who found the displacement of the Al_2O_3 surface hydroxyls by fluorine, which then proceeded to react with the Al_2O_3 exothermically. Using thermo-equilibrium analysis software REAL Code [57], the following major products were established as forming from an Al_2O_3/ C_2F_4 reaction: CO, AlF_3, Al_2O_3. These results match well with Chaudhuri and Losada [51] whose molecular modeling results predicted the formation of an aluminum fluoride compound and a carbon based compound. The Al_2O_3/ C_2F_4 reaction manifests itself as the 1st exotherm. Initially observed by Osborne and Pantoya[52] and coined pre-ignition reactions (PIR), these initial exotherms have been linked to the formation of fluorine radicals that react with the Al_2O_3 shell at high temperatures, forming as part of its products aluminum fluoride (AlF_3), similar to the present results. The exotherms circled in Fig.13, are identified to be PIRs. The longer chains manifest the PIR behavior. These chains are less stable because they require less energy to break bonds and have higher fluorine concentration [56].

The onset of the PIR is not consistent in all cases; Fig.13 shows earlier for the Al/P3 and progressively later for the increasing chain lengths. This presents a potential correlation between chain length and fluorine concentration to the PIR onset. This observation is consistent with the work of Dean and Pantoya [58] that found a

correlation between fluorine concentration and the onset of the PIR. In this study, not only do the chains differ in length but also in fluorine concentration such that these two coupled parameters play a significant role in the existence and behavior of the PIR in all composites. It is noted that all mixtures are prepared to the same stoichiometry such that fluorine concentration is a function of the PTFE chain length alone.

In regards to the two samples not showing PIRs, Fig.13 shows both have an initial mass loss. Therefore, instead of fluorinating the Al_2O_3 to create PIRs, the fluorine escapes in the case of the two shorter chained polymers and no PIRs are exhibited. This behavior could be due to increased mobility of the fluoropolymer and decreased density such that the fluorine is no longer in proximity of the Al_2O_3 and finds an easier path of escape instead of reaction. The longer chains show no mass loss in that region but a distinguishable PIR. The longer chains with reduced mobility promote fluorine interaction with the Al_2O_3 such that the PIR reaction is favored. The reaction of fluorine with Al_2O_3 is also confirmed in comparing the mass loss and thermal behaviors of the composites versus the PTFE samples alone. The mass loss found in the composites is a fraction of the loss in the PTFE tests, confirming that more fluorine reacts with the Al_2O_3 and remains in the condensed phase.

From Table 4 there is a correlation between PIR and the heat of combustion, where the earlier PIR onsets show larger heat of combustion for both exotherms indicating both improved surface interactions as well as improved core interactions. Table 4 suggests an optimal chemistry in Al/P3 that promotes improved thermal behaviors and lower PIR onsets.

Figure 15 shows flame speeds for the composites that all have the same PTFE particle size. Flame speed is a strong function of particle size and many studies show that decreased particle sizes, with both fuels and oxidizers, exhibit improved reactivity due to increased specific surface area and decreased interstitial distances [5, 7, 59, 60]. For this reason, only the flame speeds for PTFE composites with comparable particle sizes have been examined, namely: Al/P2, Al/P3 and Al/P5. The results show for composites that exhibit a PIR (i.e., Al/P3 and Al/P5), flame speeds are significantly higher in comparison to the non PIR composite. All reactions show flame speeds greater than 10 m/s and therefore they all correlate to the melt dispersion mechanism (MDM) yet composites showing PIRs and earlier onset of PIRs exhibit accelerated flame speeds. Kappagantula et al[24] studied two different chemistries of surface functionalized Al mixed with MoO3 and noted a PIR onset temperature differential correlated with a faster flame speed, where the earlier onset proved the faster flame. This study showed that flame speed may be correlated to early reaction kinetics and suggested that controlling the PIR may result in affecting the flame speed. In contrast the present study examined Al and PTFE particles with same chemistry and particle size yet PTFE varied in chain length, and found flame speeds in the MDM range (>10 m/s). The flame speeds reach a maximum of 198 m/s and the composites showing a PIR are above 100 m/s while the composite not showing a PIR is well below 100 m/s. With the consistency in particle size, these results suggest that the PIR may promote a more complete MDM activation in comparison to that of the non PIR composite, such that there is a drastic difference in flame speeds. This process is explained by focusing on the interaction of the fluorine and the Al_2O_3. Sarbak et al.[9, 26] reported infra-red

spectroscopy (FTIR) results that confirmed the existence of hydroxyls on the Al_2O_3 surface and further showed that when in the presence of fluorine, the fluorine replaces the hydroxyls on the surface. The process is illustrated in Figure.16 and shows how the fluorine exothermically dislodges the hydroxyl.

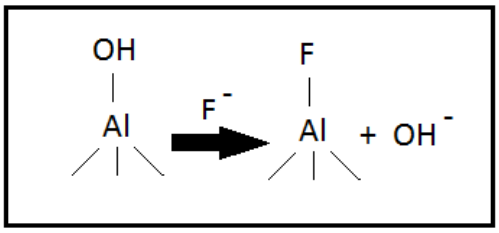

Figure 16: An illustration of how fluorine dislodges hydroxyls on the Al2O3 surface [9].

This leads to formation of Al-F surface structures on the Al_2O_3 perimeter[26]. This agrees with Langmuir[61] who emphasized that these chemical adsorption reactions involve the formation of single layer around the existing one. Therefore the PIR sets up an added layer that encapsulates the Al_2O_3 and therefore the Al core. Fluorination has previously been found to induce MDM, even up to the micron particle size[6]. Essential for the MDM to take place is that the shell remains intact long enough for the core to melt, which induces increased pressures and then followed by spallation of the shell [6, 10, 24]. Therefore the formation of Al-F on the surface of the Al_2O_3 provides the added support for the shell that it does not receive without the presence of fluorine. This added support allows for more of the Al core to melt prior to the shell breaking, which promotes a more complete MDM activation and increased flame speeds.

Results shown in Table 5 indicate that the rate of gas generation was fairly consistent for all composites and exhibited only minor deflections. From these

consistent observations and findings that higher gas concentrations did not correlate with higher flame speeds, convection does not overpower the chemical kinetics and may be the key promoting MDM and high flame speeds.

Conclusions

Thermal analysis experiments were coupled with flame speed measurements for composites containing 80 nm diameter Al particles and PTFE samples with varying chain lengths and molecular weights. Results showed that exothermic pre-ignition reactions (PIRs) were exhibited by longer chained PTFE samples but not for the shorter chained PTFE samples. These exothermic PIRs are as a result of fluorine dislodging hydroxyls on the Al_2O_3 surface. Composites with earlier PIR onsets exhibited higher heats of combustion for both PIR and main reaction, in comparison to those with later PIR onsets. The Al+PTFE flame speeds corresponding to samples that exhibited a PIR are significantly higher than when the PIR was not observed. It is theorized that the surface chemistry associated with the PIR promotes activation of the melt dispersion reaction mechanism in comparison to the composites not exhibiting a PIR. This is due to the formation of Al-F surface structures on the Al_2O_3 shell surrounding the Al core that may improve the integrity of the shell for longer than the Al_2O_3 shell on its own. Overall, the Al+PTFE sample that exhibited the earliest PIR onset, also exhibited the highest heat of combustion and fastest flame speed. These findings suggest that tailoring the molecular structure of PTFE can allow for tailored reaction kinetics and surface chemistry that can be manipulated to control the overall reactivity of aluminum. Overall this study shows there is a link between the molecular

level exothermic surface chemistry associated with alumina and the overall reactivity of aluminum particles.

CHAPTER 4:

EFFECTS OF IODINE PENTOXIDE DCOMPOSITION FRAGMENTS ON EXOTHERMIC ALUMINUM SURFACE REACTIONS

Abstract

A pre-ignition reaction (PIR) once thought to be unique to aluminum (Al) and fluorine based oxidizer reaction is observed for aluminum and an iodine containing oxidizer. This pre-ignition reaction is exothermic and preceeds the main exothermic reaction corresponding to aluminum combustion. For the aluminum and iodine oxide system, exothermic surface chemistry was recently predicted for I-O fragments forming bridge bonds with the alumina passivation shell using first principle calculations, but now has been observed experimentally. Differential Scanning Calorimetry (DSC) and Thermogravimetric analysis (TG) were used to assess aluminum and iodine pentoxide (I_2O_5) powder mixtures. Various equivalence ratios were examined and found to affect the PIR onset temperature. Prior to this work PIR have been attributed solely to surface reactions of the halogen with the Al_2O_3 surface, but results show the PIR for $Al+I_2O_5$ requires both surface and core reactions to establish a PIR and a minimum activation energy is necessary for PIR production.

Introduction

The majority of recent interest in halogen based energetic materials, more specifically iodine containing formulations, has been motivated by the biocidal effect of iodine and the increasing threats of biological warfare[62-64]. This motivation led

to novel findings and potential applications for composites containing iodine [65-68]. Energetic materials containing a mixture of nanoparticles, both fuel and oxidizer, represent a group called Metastable Intermolecular Composites [69]. As the specific surface area of the reactants increases, there is an increase in contact between the fuel and oxidizer particles which enhances reaction rates and combustive performances [7, 12, 70]. Most of these studies have been performed with aluminum (Al) as the fuel [1, 7, 10, 70, 71]. Because Al particles are surrounded by a passivation shell of alumina that can range from 2-4 nm, the smaller Al particle size leads to alumina concentration but significantly increased ignition sensitivity and greater overall reactivity [5, 13, 59, 72]. Alumina is typically considered a dead weight in propulsion applications because it does not participate in the reaction and hinders energy propagation as a heat sink [10, 11, 28, 47, 48]. Yet, overall MICs have higher energy densities in comparison to conventional explosives and so have been extensively studied for their potential uses in primers, explosives and propellants [71, 73, 74]. Information and understanding of their reaction kinetics enables tailoring reactants towards a specific application.

The MIC of interest in this work is aluminum (Al) and iodine pentoxide (I_2O_5). These composites have been documented to attain speeds of up to 2000m/s, maximum peak pressures reaching 11 MPa (m = 0.5g) and with a substantially high heat of combustion 6.22 kJ/g in comparison to other thermite reactions: such as Al/CuO (4.09 kJ/g), Al/MoO_3 (4.72 kJ/g) and Al/Fe_2O_3 (3.97 kJ/g) [72, 75]. Farley et al. [64] found that for heating rates of 10 $^oC\ min^{-1}$, micron sized particle composites of Al+I_2O_5 showed no reaction while the nano-composite counterpart produced a complex multistep reaction. The nano-scale particles with increased specific surface area

promoted reaction kinetics that otherwise were not detectable with micron scale particles. Molecular dynamic simulations performed by Chaudhuri et al. [76] show a complex multistep reaction that is as a result of I_2O_5 dissociation fragments that exothermically react with Al and its oxide shell. These fragments including IO_2, IO_3 and I_2O_3, require specific adsorption energies (i.e., -211kJ/mol per bond) to form bridge bonds with the Al fuel [76]. These calculations suggest that exothermic surface chemistry in Al + I_2O_5 reactions should be observable.

Osborne and Pantoya [52] studied the Al combined with polytetrafluoroethylene (PTFE) and observed a pre-ignition reactions (PIR) associated with the formation of fluorine radicals that react with the Al_2O_3 shell at high temperatures, forming as part of its products aluminum fluoride (AlF_3). They deduced that the fluorine played a role in the promoting exothermic surface reactions in the Al_2O_3 shell. Fluorine and iodine are highly electronegative elements and may exhibit similar halogen related behaviors when interacting with aluminum particles. The objective of this study is to resolve functional reaction kinetics associated with the Al+I_2O_5 system. This will be achieved by characterizing a baseline behavior of the composite and then studying the composite behavior at varying heating rates and equivalence ratios. With the majority of previous Al+I_2O_5 studies focusing on slower heating rates [63, 64, 68, 76]coupled with the predictions of exothermic surface chemistry [64, 76], examining higher heating rates may lead to the identification of exothermic surface chemistry. Also, varying equivalence ratios allows for an observation of the effects of fuel concentration on the behaviors of these composites. This allows for improved understanding of the composites thermal kinetic behaviors.

Materials and Methods

The aluminum (Al) powder was supplied by NovaCentrix (Austin, TX), with an average particle diameter of 80 nm with 80% Al purity and 20% alumina (Al_2O_3) passivation shell. The iodine pentoxide (I_2O_5) was procured from Sigma Aldrich (St. Louis, MO) at 99% purity. The Al + I_2O_5 mixtures were prepared at varying equivalence ratios ranging from 0.8 to 1.2 (i.e., fuel lean to fuel rich). Themeasured powders were suspended in a hexane solution then placed in a Misonix S3000 sonicator and sonicated for 1 min duration cycling 10 s on and 10 s off. The cycling program avoids damage to the oxide shell during this intimate mixing process. Post sonication the mixtures were poured into a Pyrex® dish and the hexane evaporated while in a fume hood. The mixed powder was then reclaimed for further experimentation.

Reaction Kinetics

Simultaneous Thermal Analysis (STA) was performed using a Netzsch STA 409 differential scanning calorimeter and thermogravimetric analyzer (DSC/TGA). The samples were programmed to be heated from 30-800 ^oC at a rate of 25 $^oC\ min^{-1}$ in an argon environment. Temperature calibrations for the instrument were performed using melting of a set of metal standards resulting in a temperature accuracy of ±1 ^oC. Platinum crucibles with alumina liners were used and contained 3 mg of sample during testing. Tests were performed in an argon environment where the STA column was evacuated to 1 x 10^{-4} atmospheres using a Pfeiffer model TMU turbo pump and then backfilled and purged with argon at a flow rate of 70 mL min^{-1} for the remainder of the cycle. Sintering can occur during heating and melting, ultimately affecting heat

transfer in the DSC measuring head. To insure consistency, repeatability and minimize artifact alterations of results, three experiments were performed for each sample. The data was analyzed using the NETZSCH Proteus Thermal Analysis software package.

Further STA experimentation was performed analyzing samples heated to 800 ^{o}C at 10, 20, and 40 ^{o}C min^{-1}. Activation energy was calculated using an isoconversion method presented by Starink [3] and shown in Eq. (1).

$$ln\left(\frac{B}{T_P^{1.95}}\right) = \frac{E_a}{RT_p} + ln\, A \qquad (1)$$

From Eq.(1), B is the heating rate, T_p is the exothermic peak temperature, A is a pre-exponential factor, E_a is activation energy and R is the universal gas constant and $B/T_p^{1.95}$ approximates the reaction rate.

The activation energy E_a (kJ/mol) can be found by plotting $\ln(B/T_p^{1.95})$ as a function of $(1/RT_p)$ and taking the slope of the line.

Results and Discussion

The heat flow and mass change results for pure I_2O_5 are presented in Fig.17. The heat flow DSC scale axis is representative of the energy change as a function of temperature and measured in units of mW-mg^{-1}. The mass loss TG% axis is representative of the mass change as a function of temperature. Mass loss is usually associated with drying, phase change or gas produced during reaction. Iodine pentoxide is extremely reactive and known to react with moisture in air upon exposure [64]. Iodic acid, HIO_3, is formed as a result and this process is reversed during heating as indicated by the endotherm observed at 200 ^{0}C [64]. The various stages of

dissociation are marked on Fig. 17 at the points where the heat flow lope changes (i.e., Stages A-D).

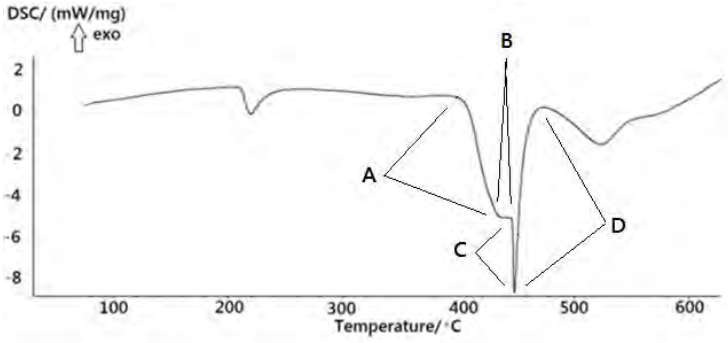

A.

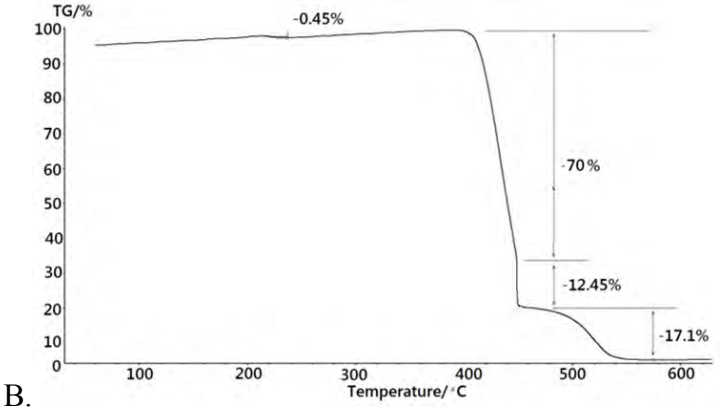

B.

Figure 17. Graphs show STA data of pure I_2O_5 in an argon environment at a heating rate of 25 $^oC\ min^{-1}$. A. heat flow reaction stages are marked A-D; and, B. mass loss behavior.

The hydroxyl decomposition process can be described by Eq. (2).

$$3HIO_3 \rightarrow HIO_3 \cdot I_2O_5 \rightarrow 1.5I_2O_5 \quad (2)$$

The mass loss at 220 ^{0}C coincides with an endotherm, and is indicative of the loss of bonded hydroxyls from I_2O_5. There is a slight dip in the heat flow that begins at approximately 300^{0}C, corresponding to the initial stages of I_2O_5 decomposition. Further I_2O_5 decomposition is observed at approximately 400 ^{0}C, where I_2O_5 dissociates into the gas phase and a 100% mass loss is observed. As shown in Fig.17 dissociation for this material is a complex multistage process. It is initiated by *Stage A* where 70% of mass is lost and the process is endothermic. This is followed by *Stage B*

where a slight exothermic process causes plateauing in the heat flow while the mass loss rate remains constant. *Stage C* shows a sharp endotherm that is exactly coincident with a significant increase in mass loss rate. A substantial change and increase is observed in *Stage D* representative of an exothermic reaction. This complex process has been previously observed yet is not well understood or thoroughly explained [64]. The I_2O_5 global decomposition reaction is shown by Eq. (3).

$$I_2O_5 \rightarrow I_2 + 2.5O_2 \tag{3}$$

The elementary reactions and stages in Fig.1 may be explained using first-principles and condensed-phase periodic density functional theory (DFT) analyses performed by Chaudhuri et al. [76]. Their simulations analyzed both the gas and solid phases of Al-I_2O_5 elementary reactions under the assumption Al particles were encapsulated with an Al_2O_3 shell and that exothermic interface reactions were taking place upon activation [76]. Interface adsorption (exothermic) and I-transfer (endothermic) processes were calculated [76]. Some decomposition kinetics are summarized in Table 6 and can be applied here to explain the exothermic and endothermic behaviors seen in Fig.17. The reactions in Table 6 where O_2 is produced post dissociation are all exothermic and have a negative enthalpy.

Table 6. Dissociation processes reported in [13] that correlate with endothermic and exothermic behaviors observed in the I_2O_5 STA (i.e., Fig. 17).

Reaction Stage	**Dissociation**	**Δ_r H (kJ/mol)**	**Onset Temperature**
Stage A Endotherm	$I_2O_5 \rightarrow IO_2 + IO_3$	37.8	405°C
Stage B Exotherm	$\rightarrow I_2O_3 + O_2$	-12.0	432°C
Stage C Endotherm	$\rightarrow IO_2 + IO$	23.2	447°C
Stage D Exotherm	$\rightarrow I_2 + O_2$	-25.8	450°C

The endothermic behavior observed in *Stage A* of Fig. 17 is associated to the first I_2O_5 decomposition stage as shown in Table 6, followed by an exothermic *Stage B*, endothermic *Stage C* and a final exotherm at *Stage D*.

Figure 18 presents the heat flow (DSC) and mass loss (TG) results for Al + I_2O_5 at an equivalence ratio (ER) of 1.0 (i.e., stoichiometric).

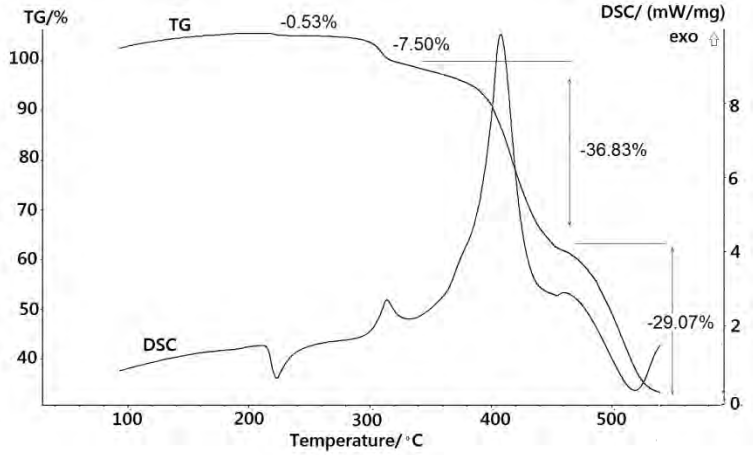

Figure 18. Heat flow and mass loss curves from DSC/TG measurements of Al/I_2O_5 in an argon environment at a heating rate of 25 °C min^{-1} .

Consistent in Figs. 17 and 18 the initial hydroxyl loss at 220 ^{o}C is observed as a small endotherm. Following, Fig.18 presents a small exotherm at approximately 320 ^{o}C, followed by a bigger exotherm at approximately 405 ^{o}C and then a small endotherm at 450^{o}C. It is noted that the heat flow curves in Figs 17 and 18 are essentially inverted above 300 ^{o}C such that areas showing exotherms in Fig. 17 are showing endotherms in Fig. 18, and vice versa. Therefore, reactions occur at the stages of I_2O_5 dissociation. The main exotherm appears to include *Stages A-B* dissociations while *Stages C-D* corresponds to the endotherm and exotherm at approximately 447 and 450^{o}C. These reactions all occur below the melting temperature for Al (660^{o}C) such that Al is in the solid phase. The Al + I_2O_5 mass loss pattern in Fig. 18 is similar to the pure I_2O_5 mass loss pattern in Fig. 17. Specifically, the initial hydroxyl mass loss is shown at approximately 220^{o}C and the changing rates of mass loss between 400-500^{o}C are repeated. All other heat flow behaviors result from adding Al to the mix. For example, a small exotherm occurs at 300 ^{o}C where no I_2O_5 dissociations were observed. This exotherm resembles an observation by Osborne and Pantoya [52] who worked with fluorine and aluminum. They observed a similar small exotherm prior to the main Al reaction and coined it a pre ignition reaction (PIR). They showed that the alumina shell surrounding the Al particle was fluorinated by the fluoride ions from polytetrafluoroethylene (PTFE) decomposition, and that this interaction was responsible for the exothermic PIR. The first exotherm shown in Fig. 18 will now be referred to as a PIR exotherm.

This PIR exotherm corresponds to a reaction involving a halogen and, yet is not the main exothermic reaction as indicated by the 2nd exotherm in Fig. 18. In the

temperature region of the PIR, I_2O_5 has not begun dissociation as shown in Fig. 17, therefore the PIR exotherm would be as a result of kinetics associated with aluminum. Farley et al.[77] found that I_2O_5 and its decomposition fragments adsorb strongly to alumina via bridge bonds and that the adsorption energy is strongly exothermic at 423 kJ/mol for a single I_2O_5 molecule. With the adsorption of iodine to Al_2O_3 the mass loss observed concurrently with the PIR in Fig. 18 is explained by the oxygen released from I_2O_5 dissociation. It is commonly understood that oxide surfaces are covered with hydroxyls as a result of atmospheric conditions. The adsorption process responsible for the PIR has I_2O_5 exothermically dislodging hydroxyls on the Al_2O_3 surface and forming I-O-Al bridge bonds requiring an adsorption energy of 211 kJ/mol per bond formed [77].

To confirm this PIR behavior associated with I_2O_5 and its fragments reacting with Al_2O_3, a mixture of Al_2O_3 + I_2O_5 was examined for the same conditions as the Al + I_2O_5 in Fig. 2. This analysis isolates reaction between the Al_2O_3 shell and I_2O_5 and Fig. 19 presents the results.

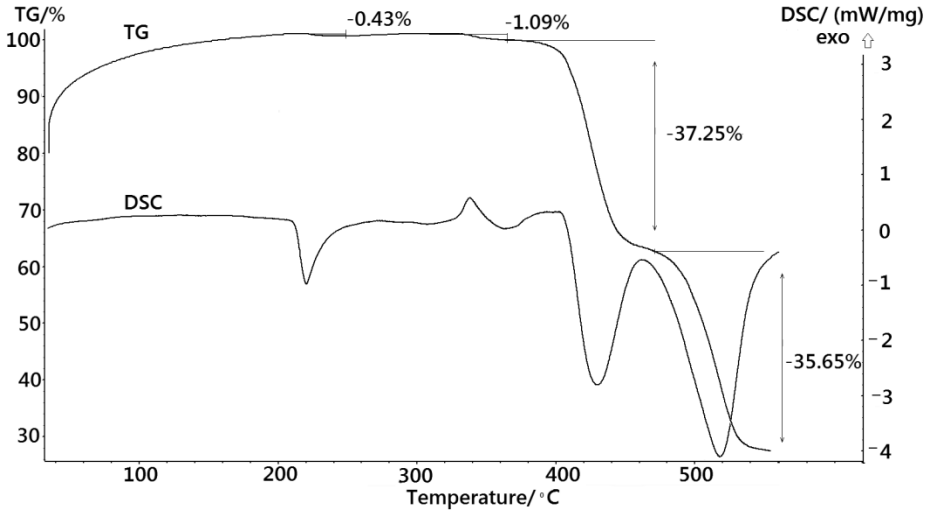

Figure 19. Heat flow and mass loss curves from DSC/TG measurements of Al_2O_3 + I_2O_5 in an argon environment at a heating rate of 25 $^oC\ min^{-1}$.

Figure 19 shows a PIR is present in the same temperature range as in Al+I_2O_5 shown in Fig. 18. Due to the oxygen inertness of Al_2O_3 at these temperatures, the exotherm can only be attributed to the bridge bonds forming between Al_2O_3 and I-O dissociation fragments. Following the PIR, no major exotherm is observed, instead two successive endotherms with the latter being larger than the first. Endothermic behavior in the 420 ^0C range is consistent with mass loss in all TG figures (Figs 17B, 18, 19) corresponding to I_2O_5 decomposition. As observed in Figs. 17B-19 there is a second endotherm attributed to the final stage of mass loss. This second endotherm is much larger in Fig. 19 in comparison to Fig. 17 and 18. The calculated heats of combustion and melting for Fig. 17-19 are presented in Table 7.

Table 7: Quantitative assessment of the heating and melting peaks in Figs 17-19.

	PIR $\Delta_r H$	Main Exotherm $\Delta_r H$	1st Endotherm $\Delta_r H$	2nd Endotherm $\Delta_r H$
Figure 1	0 J/g	0 J/g	501.7 J/g	106 J/g
Figure 2	19.98 J/g	434.4 J/g	0 J/g	151.7 J/g
Figure 3	14.04 J/g	0 J/g	179.8 J/g	307 J/g

Dreizin et al. [47] found that the amorphous Al_2O_3 shell begins significant growth from 300 ^oC and then undergoes a phase change from amorphous Al_2O_3 to γ Al_2O_3 when it reaches critical thickness (~4nm) in the 500-550 ^oC range. This phase change may be responsible for the greater endotherm in Fig. 19 in comparison to Figs. 17 and 18. The higher density associated with γ-Al_2O_3 nanocrystallites may promote enhanced bonding behavior [47].

In Fig. 19, one exothermic onset at approximately 318^oC is found which coincides with the PIR in Fig.18 but was not observed in Fig. 17. The element present in composites showing PIR in Figs. 18 and 19 that is not in the composite for Fig. 17 is Al_2O_3, such that the PIR is a result of iodination of alumina and the formation of I-O-Al bonds in coherence with calculations by Chaudhuri et al. [76].

Further experiments were performed for varying equivalence ratios and the effect on the PIR. A fuel rich 1.2 mixture was studied along with a fuel lean 0.8 mixture, and the heat flow results are presented in Fig. 20.

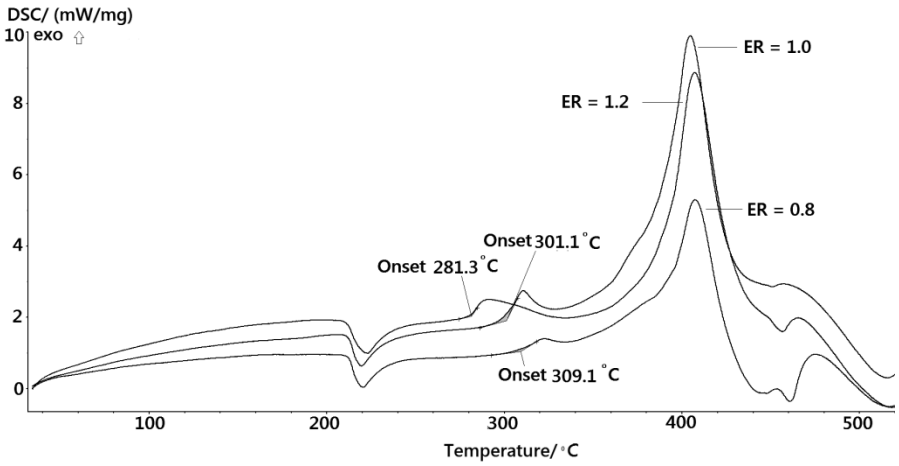

Figure 20. Heat flow curves from DSC measurements of Al + I2O5 in an argon environment at a heating rate of 25 °C min^{-1} and for varying equivalence ratios (ER).

Figure 20 shows a PIR in all cases. A difference is observed in the onsets of these PIRs: the fuel rich mixture has the lowest onset temperature (i.e., 281.3 °C) while the fuel lean mixture has the highest onset temperature (i.e., 309.1 °C). This leads to a potential concentration dependent behavior similar to observations by Dean and Pantoya [58] who found similar correlations between fluorine concentration and PIR onset. The fuel rich mixtures have more Al and therefore more Al_2O_3 which may allow for increased surface area induced reaction between the alumina shells and I_2O_5 leading to earlier observed PIRs. Therefore there appears to be a concentration factor coupled with the adsorption of I_2O_5 dissociating fragments to the Al_2O_3 surface that affects the PIR behavior. To investigate how these parameters both play a role the PI, further testing was performed with a single stoichiometry analyzed at varying heating rates.

A literature search shows that only a couple of heat flow and mass loss studies of Al+I_2O_5 have been performed and all did not observe PIR [64, 77]. These studies examined heating rates between 2-10 °C min^{-1}. Therefore, similar tests were performed

to extend to higher heating rates at 10, 20 and 40 ^{o}C min^{-1} and compared with the 25 ^{o}C min^{-1} results shown in Figs.17-20. Figure 21 presents the results for thermal behavior of Al+I_2O_5 at varying heating rates.

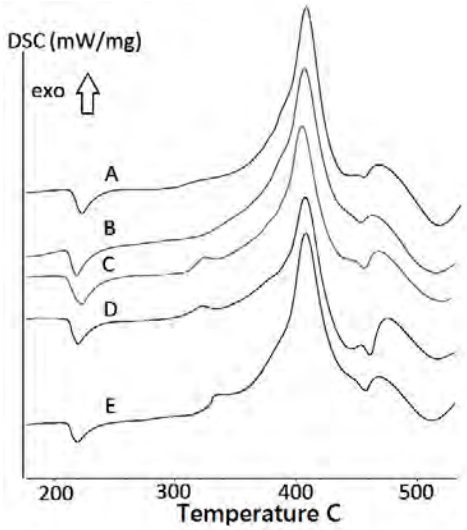

Figure 21. The effects of vary heating rates: A –10, B – 20, C – 25, D – 30, and E – 40 ^{o}C min^{-1} for composite at 0.8 ER examined in an argon environment.

Figure 21 shows that no PIR is observed until 25 ^{o}C min^{-1} heating rate and then PIR behavior observed at higher heating rates. If the PIR was simply a matter of I_2O_5 fragments interacting with the alumina surface then the lower heating rates would exhibit similar behaviors as the higher heating rates; but that is not observed in Fig. 21. Even though surface interactions contribute to the exothermicity of the PIR [52, 64, 76], there appears to be more to the PIR than just surface reactions. The varying parameter in Fig.21 is the heating rate and so its effects could explain the presence or lack of PIR.

For the varied heating rate, the activation energy was calculated as 1.43 kJ/g (from Eq. (1)) correlated to the Al_2O_3 and I_2O_5 fragments reaction. The activation

energy for Al and I_2O_5 fragments (main exotherm) was calculated and found to be 1.83 kJ/g which is comparable to the value obtained by Farley et al.[77] found to be 1.79 kJ/g. For diffusion reactions, Al and oxygen species diffuse toward each other through the oxide shell [78, 79]. Three forces take part in this action: frictional force (resistance to moving ion), diffusive force (dependent on concentration) and electrostatic force (interaction between ions)[80]. The equations correlating to these forces are presented in [80] and repeated here in Eqs. (4-6).

$$F_{es} = -\frac{dU_{es}}{dr} \tag{4}$$

$$F_d = -\frac{\boldsymbol{k}T dc_B}{c_B dr} \tag{5}$$

$$F_r = -f_B \frac{dr}{dt} \tag{6}$$

In these equations, U_{es} is the electrostatic potential, C_B is the concentration, f_B is frictional coefficient, r is the depth into the surface, T is the temperature, k is the thermal conductivity and dr/dt is the diffusive velocity [80]. These forces are combined to form the diffusive flux (J_B) which refers to the number of ions passing through the surface. The equation for J_B is derived in [80] and given by Eq. (7).

$$J_B = \frac{4\pi r^2 kT}{f_B}\left(\frac{dc_B}{dr} + \frac{c_B\, dU_{es}}{kT\, dr}\right) \tag{7}$$

$$= -\frac{dr}{dt} 4\pi r^2$$

Increasing the heating rate increases the temperature gradient between the outside surface and the core, and higher temperatures cause an increase in molecular kinetic energy represented by Eq. (8).

$$K_{energy} = \frac{1}{2} m \left(\frac{dr}{dt}\right)^2 \quad (8)$$

Therefore if heating rate is increased, kinetic energy is increased and diffusive velocity is increased in accordance with Eq. (6). An increase in diffusive velocity relates to an increase in diffusive flux and promotes increased reaction of iodine and Al_2O_3. Based on the deductions above, the electrostatic component of diffusive flux and the ionic nature of this composite, I_2O_5 fragments also diffuse into the Al_2O_3 shell. Therefore, the Al_2O_3 surface is not only interacting with oxygen and the I_2O_5 fragments, there is a diffusion of oxygen and some ionic I_2O_5 fragments into the oxide layer.

Based on Fig. 21 increasing heating rate beyond the threshold where the PIR is observed (i.e., 25 $^oC\ min^{-1}$) results in a consistent PIR observation. For diffusion controlled reactions, increasing heating rates increases diffusion velocities of the oxygen towards the Al and of the Al towards the oxygen, but it also increases the diffusion flux of other ionic elements. Therefore there appears to be a balance such that beyond a threshold heating rate the concentration of ionic elements diffusing into the shell would balance the oxygen to Al diffusion and exhibit a consistent PIR. It is also noted that slower heating rates may reach this threshold such that concentration of I_2O_5 to Al_2O_3 interaction is sufficient for PIR, the reaction may be simultaneous with the main combustion reaction and therefore cannot be observed. These observations suggest that not just surface reactions are responsible for the PIR, but core interactions as well.

Conclusion

Exothermic surface chemistry associated with the alumina passivation shell and iodine containing species was identified prior to the main aluminum combustion reaction. Powder composites composed of nano-scale aluminum particles passivated with an alumina shell and iodine pentoxide particles were examined using Differential Scanning Calorimetry (DSC) and Thermogravimetric analysis (TG). A multi-staged endothermic/exothermic behavior unique to I_2O_5 was observed and explained using predicted molecular dynamics models that result from multiple I_2O_5 dissociation fragments. A pre-ignition reaction (PIR) once thought to be unique to nano-Al/PTFE mixtures was revealed for the Al/I_2O_5 and Al_2O_3/I_2O_5 mixtures, as well as fuel rich and fuel lean mixtures. Correlations with the diffusive flux showed that PIR is dependent on both the concentration and activation energy. Adsorption of I_2O_5 fragments to the Al_2O_3 surface coupled with diffusion of ionic I_2O_5 fragments in to the Al_2O_3 shell, were found to play a significant role in the production of PIRs. The effect of varying equivalence ratios did not affect the production of a PIR but rather its onset temperature. The fuel rich mixtures show lower onset temperatures and the fuel lean mixtures showed higher onset temperatures such that the PIR was concentration dependent. These are impactful findings because the alumina passivation shell is typically considered dead weight and a heat sink in combustion reactions, but is shown here to participate exothermically in the reaction when combined with an iodine containing oxidizer.

CHAPTER 5:
CONCLUSION

Aluminum (Al) fueled reactions show improved combustion efficiency when environmental oxygen is minimized, and Al reaction with the solid oxidizer is encouraged. Introducing an oxygen scavenging additive, hafnium hydride (HfH2), into the reaction creates oxidation competitions that improve combustion. Specifically, HfH2 reacts with atmospheric oxygen just prior to Al ignition such that improved heat of combustion up to 12% was achieved with 10% HfH2 addition. Beyond 10%, HfH2 competes with Al for reaction with the solid oxidizer producing diminished heats of combustion. Improved combustion behavior is indeed feasible and limiting the oxygen available for reaction to that contained in the solid oxidizer has been observed to be a successful method of achieving greater overall heat of combustion. When observing detonation initiation, HfH2 was shown to significantly increase the energy available from the Al+ CuO composite in detonation ignition tests. The improvement is attributed to reaction kinetics that forces Al to react with CuO instead of oxygen from the environment. These results have impact on ballistic applications where thermite powders are used as primers in confined environments. Specifically, tailoring the composite with an oxygen scavenging additive may promote increased chemical energy potential.

Thermal analysis experiments were coupled with flame speed measurements for composites containing 80 nm diameter Al particles and PTFE samples with varying chain lengths and molecular weights. Results showed that exothermic pre-

ignition reactions (PIRs) were exhibited by longer chained PTFE samples but not for the shorter chained PTFE samples. These exothermic PIRs are as a result of fluorine dislodging hydroxyls on the Al_2O_3 surface. Composites with earlier PIR onsets exhibited higher heats of combustion for both PIR and main reaction, in comparison to those with later PIR onsets. The Al+PTFE flame speeds corresponding to samples that exhibited a PIR are significantly higher than when the PIR was not observed. It is theorized that the surface chemistry associated with the PIR promotes activation of the melt dispersion reaction mechanism in comparison to the composites not exhibiting a PIR. This is due to the formation of Al-F surface structures on the Al_2O_3 shell surrounding the Al core that may improve the integrity of the shell for longer than the Al_2O_3 shell on its own. Overall, the Al+PTFE sample that exhibited the earliest PIR onset, also exhibited the highest heat of combustion and fastest flame speed. These findings suggest that tailoring the molecular structure of PTFE can allow for tailored reaction kinetics and surface chemistry that can be manipulated to control the overall reactivity of aluminum. Overall this study shows there is a link between the molecular level exothermic surface chemistry associated with alumina and the overall reactivity of aluminum particles.

Differential Scanning Calorimetry (DSC) and Thermogravimetric analysis (TG) were used to assess Al/I_2O_5 and Al_2O_3/I_2O_5 composite mixtures. A multi-staged endothermic/exothermic behavior unique to I_2O_5 was observed and explained using predicted molecular dynamics models. This process is as a result of the multiple I_2O_5 dissociation fragments. A pre-ignition reaction (PIR) once thought to be unique to nano-Al/PTFE mixtures was revealed for the Al/I_2O_5 and Al_2O_3/I_2O_5 mixtures, as well

as fuel rich and fuel lean mixtures. Correlations with the diffusive flux showed that PIR presence and behavior is dependent on but not limited to both the concentration and activation energy. Adsorption of I_2O_5 fragments to the Al_2O_3 surface coupled with diffusion of ionic I_2O_5 fragments in to the Al_2O_3 shell, were found to play a significant role in the production of PIRs. The effect of varying equivalence ratios did not affect the production of a PIR but rather its onset temperature. The fuel rich mixtures show lower onset temperatures and the fuel lean mixtures showed higher onset temperatures. This showed a behavior with a concentration dependence, which was confirmed through the assessment of the diffusive flux. These are impactful findings because they present the first time a PIR has been consistently observed with an Al/I_2O_5 composite, and presents explanations governing the behavior.

FUTURE WORK

REFERENCES

[1] E. L. Dreizin, "Metal-based reactive nanomaterials," *Progress in Energy and Combustion Science,* vol. 35, pp. 141-167, Apr 2009.

[2] F. H. Constable, "The Mechanism of Catalytic Decomposition," *Proceedings of the Royal Society London A,* pp. 355-378, 1925.

[3] M. J. Starink, "Analysis of aluminium based alloys by catorimetry: quantitative analysis of reactions and reaction kinetics," *International Materials Reviews,* vol. 49, pp. 191-226, Jun-Aug 2004.

[4] H. S. Taylor, "The Mechanism of Activation at Catalytic Surfaces," *Proceedings of the Royal Society London A,* pp. 77-86, 1926.

[5] C. E. Aumann, G. L. Skofronick, and J. A. Martin, "OXIDATION BEHAVIOR OF ALUMINUM NANOPOWDERS," *Journal of Vacuum Science & Technology B,* vol. 13, pp. 1178-1183, May-Jun 1995.

[6] V. I. Levitas, M. L. Pantoya, and K. W. Watson, "Melt-dispersion mechanism for fast reaction of aluminum particles: Extension for micron scale particles and fluorination," *Applied Physics Letters,* vol. 92, May 19 2008.

[7] B. S. Bockmon, M. L. Pantoya, S. F. Son, B. W. Asay, and J. T. Mang, "Combustion velocities and propagation mechanisms of metastable interstitial composites," *Journal of Applied Physics,* vol. 98, Sep 15 2005.

[8] A. Koch, N. Arnold, and M. Estermann, "A simple relation between the detonation velocity of an explosive and its gurney energy," *Propellants Explosives Pyrotechnics,* vol. 27, pp. 365-368, Dec 2002.

[9] Z. Sarbak, "The effect of fluoride concentration and catalyst preparation method on structural and thermal properties of CoMo/Al2O3 catalysts," *Crystal Research and Technology,* vol. 32, pp. 1007-1013, 1997 1997.

[10] B. Dikici, S. W. Dean, M. L. Pantoya, V. I. Levitas, and R. J. Jouet, "Influence of Aluminum Passivation on the Reaction Mechanism: Flame Propagation Studies," *Energy & Fuels,* vol. 23, pp. 4231-4235, Sep 2009.

[11] J. Gesner, M. L. Pantoya, and V. I. Levitas, "Effect of oxide shell growth on nano-aluminum thermite propagation rates," *Combustion and Flame,* vol. 159, pp. 3448-3453, Nov 2012.

[12] J. J. Granier and M. L. Pantoya, "Laser ignition of nanocomposite thermites," *Combustion and Flame,* vol. 138, pp. 373-383, Sep 2004.

[13] J. Y. Ahn, W. D. Kim, K. Cho, D. Lee, and S. H. Kim, "Effect of metal oxide nanostructures on the explosive property of metastable intermolecular composite particles," *Powder Technology,* vol. 211, pp. 65-71, Jul 25 2011.

[14] H. Xu, R. Li, J. Shen, G. Yang, and C. Pei, "Preparation and characterisation of nanofibrous CuO/Al metastable intermolecular composite films," *Micro & Nano Letters,* vol. 7, pp. 1251-1255, Dec 2012.

[15] M. T. Reetz, "Biocatalysis in Organic Chemistry and Biotechnology: Past, Present, and Future," *Journal of the American Chemical Society,* vol. 135, pp. 12480-12496, Aug 28 2013.

[16] K. S. Kappagantula, C. Farley, M. L. Pantoya, and J. Horn, "Tuning Energetic Material Reactivity Using Surface Functionalization of Aluminum Fuels," *Journal of Physical Chemistry C,* vol. 116, pp. 24469-24475, Nov 2012.

[17] Y. Q. Yang, S. F. Wang, Z. Y. Sun, and D. D. Dlott, "Near-infrared and visible absorption spectroscopy of nano-energetic materials containing aluminum and boron," *Propellants Explosives Pyrotechnics,* vol. 30, pp. 171-177, Jun 2005.

[18] N. Kubota and C. Serizawa, "COMBUSTION OF MAGNESIUM POLYTETRAFLUOROETHYLENE," *Journal of Propulsion and Power,* vol. 3, pp. 303-307, Jul-Aug 1987.

[19] K. Kappagantula, M. L. Pantoya, and E. M. Hunt, "Impact ignition of aluminum-teflon based energetic materials impregnated with nano-structured carbon additives," *Journal of Applied Physics,* vol. 112, Jul 15 2012.

[20] E. P. Collins, M.L.; Skelton, B.R.; Green, M.J.; Daniels, M., "Ignition Sensitivity and Electrical Conductivity of a Composite Energetic Material with Conductive Nanofillers," *Journal of NanoTechnology,* 2013.

[21] E. M. Hunt and M. L. Pantoya, "Impact sensitivity of intermetallic nanocomposites: A study on compositional and bulk density," *Intermetallics,* vol. 18, pp. 1612-1616, Aug 2010.

[22] V. I. Levitas, B. W. Asay, S. F. Son, and M. Pantoya, "Melt dispersion mechanism for fast reaction of nanothermites," *Applied Physics Letters,* vol. 89, Aug 14 2006.

[23] V. I. Levitas, B. W. Asay, S. F. Son, and M. Pantoya, "Mechanochemical mechanism for fast reaction of metastable intermolecular composites based on dispersion of liquid metal," *Journal of Applied Physics,* vol. 101, Apr 15 2007.

[24] V. I. Levitas, B. Dikici, and M. L. Pantoya, "Toward design of the pre-stressed nano- and microscale aluminum particles covered by oxide shell," *Combustion and Flame,* vol. 158, pp. 1413-1417, Jul 2011.

[25] V. I. Levitas, M. L. Pantoya, and B. Dikici, "Melt dispersion versus diffusive oxidation mechanism for aluminum nanoparticles: Critical experiments and controlling parameters," *Applied Physics Letters,* vol. 92, Jan 7 2008.

[26] Z. Sarbak, "Effect of fluoride and sodium ions on structural and thermal properties of gamma-Al2O3," *Crystal Research and Technology,* vol. 32, pp. 491-497, 1997 1997.

[27] S. Hasani, M. Panjepour, and M. Shamanian, "The Oxidation Mechanism of Pure Aluminum Powder Particles," *Oxidation of Metals,* vol. 78, pp. 179-195, 2012/10/01 2012.

[28] M. A. Trunov, S. M. Umbrajkar, M. Schoenitz, J. T. Mang, and E. L. Dreizin, "Oxidation and melting of aluminum nanopowders," *Journal of Physical Chemistry B,* vol. 110, pp. 13094-9, Jul 6 2006.

[29] K. P. Brooks and M. W. Beckstead, "DYNAMICS OF ALUMINUM COMBUSTION," *Journal of Propulsion and Power,* vol. 11, pp. 769-780, Jul-Aug 1995.

[30] P. E. Snyder and H. Seltz, "The Heat of Formation of Aluminum Oxide," *Journal of the American Chemical Society,* vol. 67, pp. 683-685, 1945/04/01 1945.

[31] J. A. Rodriguez, J. Y. Kim, J. C. Hanson, M. Perez, and A. I. Frenkel, "Reduction of CuO in H-2: in situ time-resolved XRD studies," *Catalysis Letters,* vol. 85, pp. 247-254, Feb 2003.

[32] R. V. Kumar, R. Elgamiel, Y. Diamant, A. Gedanken, and J. Norwig, "Sonochemical preparation and characterization of nanocrystalline copper oxide embedded in poly(vinyl alcohol) and its effect on crystal growth of copper oxide," *Langmuir,* vol. 17, pp. 1406-1410, Mar 2001.

[33] J. L. Li, T. Takeguchi, and T. Inui, "Doping effect of potassium permanganate on the performance of a copper/zinc oxide/alumina catalyst for methanol formation," *Applied Catalysis a-General,* vol. 139, pp. 97-106, Jun 1996.

[34] A. W. Miziolek, "Nanoenergetics: An Emerging Technology Area of National Importance," *AMPTIAC Quarterly,* vol. 6, pp. 43-48, 2002.

[35] O. G. Cervantes, J. D. Kuntz, A. E. Gash, and Z. A. Munir, "Heat of combustion of tantalum-tungsten oxide thermite composites," *Combustion and Flame,* vol. 157, pp. 2326-2332, Dec 2010.

[36] S. H. Fischer and M. C. Grubelich, "Theoretical energy release of thermites, intermetallics, and combustible metals," SAND--98-1176C; CONF-980728--; Other: ON: DE98005512; BR: 400403310; TRN: US200223%%671, 1998.

[37] O. A. Kubaschewski, C.B. ; Spencer, P.J., *Materials Thermochemistry*, 6 ed. Oxford: Pergamon, 1993.

[38] H. J. Reich, *Principles of Electron Tubes*: Literary Licensing, LLC, 2013.

[39] M. Ito, K. Kurosaki, H. Muta, M. Uno, K. Konashi, and S. Yamanaka, "Thermomechanical Properties of Hafnium Hydride," *Journal of Nuclear Science and Technology,* vol. 47, pp. 156-159, Feb 2010.

[40] B. Tsuchiya, Y. Arita, H. Muta, K. Kurosaki, K. Konashi, S. Nagata, and T. Shikama, "Thermal transport properties of hafnium hydrides and deuterides," *Journal of Nuclear Materials,* vol. 392, pp. 464-470, Aug 2009.

[41] M. Ito, K. Kurosaki, H. Muta, M. Uno, K. Konashi, and S. Yamanaka, "Thermal Conductivity of Hafnium Hydride," *Journal of Nuclear Science and Technology,* vol. 46, pp. 814-818, Aug 2009.

[42] W. D. Bond, "THERMOGRAVIMETRIC STUDY OF THE KINETICS OF THE REDUCTION OF CUPRIC OXIDE BY HYDROGEN1," *The Journal of Physical Chemistry,* vol. 66, pp. 1573-1577, 1962/09/01 1962.

[43] N. Ohtsu, B. Tsuchiya, M. Oku, T. Shikama, and K. Wagatsuma, "X-ray photoelectron spectroscopic study on initial oxidation of hafnium hydride fractured in an ultra-high vacuum," *Applied Surface Science,* vol. 253, pp. 6844-6847, 2007.

[44] A. N. Kornilov, I. M. Ushakova, E. J. Huber Jr, and C. E. Holley Jr, "The enthalpy of formation of hafnium dioxide," *The Journal of Chemical Thermodynamics,* vol. 7, pp. 21-26, 1975.

[45] J. Pike, S.-W. Chan, F. Zhang, X. Wang, and J. Hanson, "Formation of stable Cu2O from reduction of CuO nanoparticles," *Applied Catalysis A: General,* vol. 303, pp. 273-277, 2006.

[46] M. A. Trunov, M. Schoenitz, and E. L. Dreizin, "Ignition of aluminum powders under different experimental conditions," *Propellants Explosives Pyrotechnics,* vol. 30, pp. 36-43, Feb 2005.

[47] M. A. Trunov, M. Schoenitz, X. Zhu, and E. L. Dreizin, "Effect of polymorphic phase transformations in Al2O3 film on oxidation kinetics of aluminum powders," *Combustion and Flame,* vol. 140, pp. 310-318, 2005.

[48] M. Erickson, "REACTION VELOCITIES IN FREE STANDING ALUMINUM AND COPPER OXIDE THIN FILMS," M.S.E.E, Electrical Engineering, University of Central Florida, 2010.

[49] L. J. Parker, H. D. Ladouceur, and T. P. Russell, "Teflon and Teflon/A1 (nanocrystalline) decomposition chemistry at high pressures," in *Shock Compression of Condensed Matter-1999, Pts 1 and 2*. vol. 505, M. D. Furnish, L. C. Chhabildas, and R. S. Hixson, Eds., ed, 2000, pp. 941-944.

[50] A. Y. Dolgoborodov, M. N. Makhov, I. V. Kolbanev, A. N. Streletskii, and V. E. Fortov, "Detonation in an aluminum-teflon mixture," *Jetp Letters,* vol. 81, pp. 311-314, 2005 2005.

[51] M. Losada and S. Chaudhuri, "Theoretical Study of Elementary Steps in the Reactions between Aluminum and Teflon Fragments under Combustive Environments," *Journal of Physical Chemistry A,* vol. 113, pp. 5933-5941, May 21 2009.

[52] D. T. Osborne and M. L. Pantoya, "Effect of al particle size on the thermal degradation of Al/Teflon mixtures," *Combustion Science and Technology,* vol. 179, pp. 1467-1480, 2007 2007.

[53] K. W. Watson, M. L. Pantoya, and V. I. Levitas, "Fast reactions with nano- and micrometer aluminum: A study on oxidation versus fluorination," *Combustion and Flame,* vol. 155, pp. 619-634, Dec 2008.

[54] V. I. Levitas, "Burn time of aluminum nanoparticles: Strong effect of the heating rate and melt-dispersion mechanism," *Combustion and Flame,* vol. 156, pp. 543-546, Feb 2009.

[55] M. P. Stevens, *Polymer Chemistry: An Introduction*: Oxford University Press, 1999.

[56] T. W. G. Solomons and C. B. Fryhle, *ORGANIC CHEMISTRY, 9TH ED*: Wiley India Pvt. Limited, 2008.

[57] G. V. Belov and B. G. Trusov, "Influence of thermodynamic and thermochemical data errors on calculated equilibrium composition," *Berichte Der Bunsen-Gesellschaft-Physical Chemistry Chemical Physics,* vol. 102, pp. 1874-1879, Dec 1998.

[58] M. L. Pantoya and S. W. Dean, "The influence of alumina passivation on nano-Al/Teflon reactions," *Thermochimica Acta,* vol. 493, pp. 109-110, Sep 10 2009.

[59] M. E. Brown, S. J. Taylor, and M. J. Tribelhorn, "Fuel-oxidant particle contact in binary pyrotechnic reactions," *Propellants Explosives Pyrotechnics,* vol. 23, pp. 320-327, Dec 1998.

[60] R. A. Rugunanan and M. E. Brown, "COMBUSTION OF BINARY AND TERNARY SILICON OXIDANT PYROTECHNIC SYSTEMS .1. BINARY-SYSTEMS WITH FE2O3 AND SNO2 AS OXIDANTS," *Combustion Science and Technology,* vol. 95, pp. 61-83, 1994 1994.

[61] I. Langmuir, "The Constitution and Fundamental Properties of Solids and Liquids," *Journal of the American Chemical Society,* vol. 38, pp. 2217-2218, 1916/10/01 1916.

[62] O. K. Mulamba, E. M. Hunt, and M. L. Pantoya, "Neutralizing bacterial spores using halogenated energetic reactions " *Biotechnology and Bioprocessing Engineering,* vol. 19, 2013.

[63] B. R. Clark and M. L. Pantoya, "The aluminium and iodine pentoxide reaction for the destruction of spore forming bacteria," *Phys Chem Chem Phys,* vol. 12, pp. 12653-7, Oct 21 2010.

[64] C. Farley and M. Pantoya, "Reaction kinetics of nanometric aluminum and iodine pentoxide," *Journal of Thermal Analysis and Calorimetry,* vol. 102, pp. 609-613, Nov 2010.

[65] B. R. Clark and M. L. Pantoya, "The aluminium and iodine pentoxide reaction for the destruction of spore forming bacteria," *Physical Chemistry Chemical Physics,* vol. 12, pp. 12653-12657, 2010 2010.

[66] R. Russell, S. Bless, A. Blinkova, and T. Chen, "SPORICIDAL EFFECTS OF IODINE-OXIDE THERMITE REACTION PRODUCTS," in *Shock Compression of Condensed Matter - 2011, Pts 1 and 2*. vol. 1426, M. L. Elert, W. T. Buttler, J. P. Borg, J. L. Jordan, and T. J. Vogler, Eds., ed, 2012.

[67] R. Russell, S. Bless, and M. Pantoya, "Impact-Driven Thermite Reactions with Iodine Pentoxide and Silver Oxide," *Journal of Energetic Materials,* vol. 29, pp. 175-192, 2011 2011.

[68] S. Zhang, M. Schoenitz, and E. L. Dreizin, "Iodine Release, Oxidation, and Ignition of Mechanically Alloyed Al-I Composites," *Journal of Physical Chemistry C,* vol. 114, pp. 19653-19659, Nov 25 2010.

[69] A. W. Miziolek, "Nanoenergetics: An Emerging Technology Area of National Importance," *Advanced Materials, Manufacturing and Testing Information Analysis Center,* vol. 6, p. 43, 2002.

[70] K. B. Plantier, M. L. Pantoya, and A. E. Gash, "Combustion wave speeds of nanocomposite Al/Fe2O3: the effects of Fe2O3 particle synthesis technique," *Combustion and Flame,* vol. 140, pp. 299-309, Mar 2005.

[71] S. H. Kim and M. R. Zachariah, "Enhancing the rate of energy release from nanoenergetic materials by electrostatically enhanced assembly," *Advanced Materials,* vol. 16, pp. 1821-+, Oct 18 2004.

[72] D. D. Dlott, "Thinking big (and small) about energetic materials," *Materials Science and Technology,* vol. 22, pp. 463-473, Apr 2006.

[73] V. Hlavacek, P. Pranda, and K. Prandova, "Reactivity, stored energy, and dislocations in solid-solid reacting systems," *Chemical Engineering Communications,* vol. 192, pp. 933-940, Jul 2005.

[74] S. Valliappan, J. Swiatkiewicz, and J. A. Puszynski, "Reactivity of aluminum nanopowders with metal oxides," *Powder Technology,* vol. 156, pp. 164-169, Aug 23 2005.

[75] K. S. Martirosyan, L. Wang, and D. Luss, "Novel nanoenergetic system based on iodine pentoxide," *Chemical Physics Letters,* vol. 483, pp. 107-110, Nov 24 2009.

[76] C. Farley, M. L. Pantoya, and S. Chaudhuri, "Linking molecular level chemistry to macroscopic combustion behavior

for nano-energetic materials with halogen containing oxides," *The Journal of Chemical Physics,* vol. 139, 2013.

[77] C. W. Farley, M. L. Pantoya, M. Losada, and S. Chaudhuri, "Linking molecular level chemistry to macroscopic combustion behavior for nano-energetic materials with halogen containing oxides," *The Journal of Chemical Physics,* vol. 139, pp. 074701-8, 2013.

[78] S. Chowdhury, K. Sullivan, N. Piekiel, L. Zhou, and M. R. Zachariah, "Diffusive vs Explosive Reaction at the Nanoscale," *Journal of Physical Chemistry C,* vol. 114, pp. 9191-9195, May 27 2010.

[79] A. Rai, K. Park, L. Zhou, and M. R. Zachariah, "Understanding the mechanism of aluminium nanoparticle oxidation," *Combustion Theory and Modelling,* vol. 10, pp. 843-859, Oct 2006.

[80] L. K.J., *Chemical Kinetics*: Pearson Education, 1987.